Experimental and Computational Analysis of CO_2 Addition Reactions Relevant to Copper-Catalyzed Boracarboxylation of Vinyl Arenes: Evidence for a Phosphine-Promoted Mechanism

Notashia N. Baughman, Novruz G. Akhmedov, Jeffrey L. Petersen, and Brian V. Popp*

C. Eugene Bennett Department of Chemistry, West Virginia University, 100 Prospect Street, Morgantown, West Virginia 26506, United States.

Supporting Information Placeholder

ABSTRACT: An experimental and computational mechanistic investigation of the key carboxylation step in copper(I)-catalyzed boracarboxylation of vinyl arenes is presented here. Catalytically relevant intermediates, including a series of Cu^{I}-spiroboralactonate complexes, with electronically differentiated vinyl arenes and stabilized by the NHC ligand IPr (IPr = 1,3-Bis(2,6-diisopropylphenyl)imidazol-2-ylidine), were isolated and characterized. In situ ^{1}H NMR timecourse studies and subsequent Hammett analysis (σ_p) of carbon dioxide addition to (β-borylbenzyl)copper(I) complexes (benzyl = $CH_2Ar^{p\text{-}X}$) revealed a linear correlation with a negative rho (ρ) value. Density functional theory (DFT) calculations support a direct CO_2 insertion as the primary mechanism for electron-rich benzyl-copper carboxylation. Kinetically sluggish carboxylation of electron-poor trifluoromethyl-substituted benzyl-copper complex (benzyl = $CH_2Ar^{p\text{-}CF_3}$) was accelerated upon addition of exogenous PPh_3. Conversely, the additive inhibited reactions of electron-rich tert-butyl-substituted benzyl-copper complex (benzyl = $CH_2Ar^{p\text{-}tBu}$). These kinetic observations implied that a second carboxylation pathway was likely operative. DFT analysis demonstrated that prior binding of the electron-rich phosphine additive at (β-borylbenzyl)copper(I) yields a meta-stable intermediate that precedes an S_E-carboxylation mechanism, which is kinetically favorable for electron-deficient benzyl-copper species and circumvents the kinetically challenging direct insertion mechanism. The mechanistic picture that emerges from this complementary experimental/computational study highlights the kinetic complexities and multiple pathways involved in copper-based carboxylation chemistry.

INTRODUCTION

The synthetic utility of carbon dioxide (CO_2) has been of significant scientific interest coinciding with global discussion of greenhouse gas reduction.[1] In addition to industrial applications using CO_2, exemplified by the synthesis of urea,[2,3] several promising synthetic uses have been recognized, including the synthesis of methanol, molecular and polymeric carbonates, and other small molecules.[4,5,6] The incorporation of CO_2 into existing organic and organometallic frameworks provides a direct route to the production of carboxylates and carboxylic acids, as well as other interesting value-added products.[7] This is attractive from a pharmaceutical standpoint, as there are many existing bioactive molecules that possess the carboxylate functional group.[8,9]

Incentive to couple CO_2 with other readily available organic materials, such as unactivated alkanes and unsaturated compounds, via reductive carboxylation has led to significant advances in the field. Most carboxylation strategies rely heavily on the use of transition metal complexes[10] to gain access to desirable products such as complex carboxylic acid derivatives through a variety of C-E (E= B[11] and Sn[12]), C-H,[13] and C-X[14] bond transformations. In recent years, our research group has been interested in a relatively new class of carboxylation reactions wherein the reductant is not a hydride equivalent, but rather a heteroatom moiety (such as silicon, boron, nitrogen) termed hetero(element)carboxylation. This has been achieved predominately with copper(I) catalysis for the boracarboxylation of imines and alkynes,[15] silacarboxylation of allenes and alkynes,[16] and azacarboxylation of alkynylanilines.[17,18] In 2016, Popp and colleagues extended boracarboxylation to vinyl arenes, an important reactant class in catalytic alkene difunctionalization.[19,20] Boracarboxylation is proposed to proceed via in situ generated Cu^{I}-alkoxide complex ligated by the *N*-heterocyclic carbene (NHC) dicyclohexyl-2*H*-imidazolylidene (ICy) (Scheme 1). The method is amenable to several electron-rich and electron-neutral styrene derivatives, and it was possible to generate boron-substituted analogs of commonly prescribed nonsteroidal anti-inflammatory drugs (NSAIDs). Subsequently, more effective catalysis was achieved by our group wherein the inclusion of additives such as triphenylphosphine

Scheme 1. Proposed mechanism for the copper(I)-catalyzed boracarboxylation of vinyl arenes.

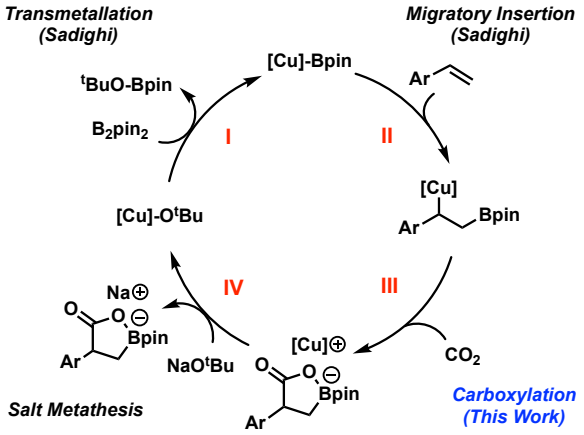

(PPh_3) provided access to electron deficient vinyl arenes, which were unreactive in the original catalytic conditions.[21] However, the role of the additive is not yet well understood. Further, despite the general success using a variety of unsubstituted vinyl arene derivatives, these methodologies are not amenable to a wide scope of other alkene substrates. We recognized that a lack of an in-depth mechanistic understanding has hindered our progress in generalizing the method.

Several previous studies support the proposed mechanism for the boracarboxylation of vinyl arenes. Sadighi and colleagues reported the synthesis and reactivity of IPrCu^{I}Bpin[22] (IPr = 1,3-Bis(2,6-diisopropylphenyl)imidazol-2-ylidine) as well as the resulting boracupration product[23] upon treatment with a series of alkene substrates (Scheme 1, Steps I and II, respectively). Despite his group demonstrating insertion of CO_2 into a number of NHC-Cu^{I} complexes,[22,24,25] carboxylation of the Cu^{I}(β-borylbenzyl) species relevant to the current study was not reported. Carboxylation of alkynes, however, has been reported by Hou, following an analogous insertion of the substrate into a Cu^{I}-Bpin bond. [15b] Several independent computational studies have detailed specific aspects of the proposed cycle, such as the role of sodium tert-butoxide (NaO^{t}Bu)[26] and the electronic and steric contributions of the ancillary ligand[27] and the boron moiety.[28] Nevertheless, direct experimental evidence in support of the proposed mechanism, remains lacking.

Herein, we present an experimental study of copper(I)-catalyzed boracarboxylation of vinyl arenes complemented by density functional theory. Successful synthesis of a series of substituted copper(I) spiroboralactonate complexes is reported, and the fluxional behavior of these compounds detected by VT ^{1}H NMR studies and corroborated computationally provides insight into how these complexes may behave under catalytic conditions. Further, the electronic impact of the arene ring was evaluated following the synthesis of several Cu^{I}(β-borylbenzyl) complexes, where it was demonstrated that increasingly electron deficient vinyl arenes undergo carboxylation at substantially slower rates. Inclusion of exogeneous electron-rich PPh_3 provided access to severely electron deficient vinyl arene substrates, and further analysis revealed multiple competing pathways are operative in the incorporation of carbon dioxide.

RESULTS AND DISCUSSION

Isolation of catalytic intermediates: Our studies of the mechanism of boracarboxylation began with attempted isolation of reactive intermediates using the catalytically competent ICyCuCl precatalyst. The proposed catalytic cycle (Scheme 1) is initiated by the generation of an active copper-alkoxide complex from ICyCuCl in the presence of sodium tert-butoxide.[19,21] To the best of our knowledge, only ICyCuO^{t}Bu[29] has been definitively characterized while catalytically relevant ICyCu^{I}Bpin and ICyCu^{I}(β-borylbenzyl) (Scheme 1, step II and III, respectively) have not been isolated. ICyCuO^{t}Bu (**1^{ICy}**) was synthesized following the literature from treatment of ICyCuCl with NaO^{t}Bu (1 equiv.).[29] Following this, attempts were made to isolate ICyCuB(pin), a presumed intermediate during catalytic reduction of CO_2 to CO.[22] Similar to previous reports, rapid decomposition of ICyCu–species was observed,[22,30] rendering isolation of ICyCu^{I}–boryl complex and subsequent reactivity studies impractical. In lieu of isolation, addition of vinyl arene to a mixture ICyCuO^{t}Bu and B_2pin_2 led to a complicated spectrum featuring an intractable mixture of products.

Given these difficulties, we turned our attention to the well-known IPr-copper system.[15,22,23] Notably, the IPrCuCl precatalyst proved ineffective in our original methodology catalyst screening,[19] making the IPr ligand a good candidate for isolation of more stable complexes. In order to understand the reactivity of Cu^{I}(β-borylbenzyl) carboxylation, we first needed to generate the insertion complexes that were reported by Sadighi.[23] IPrCuO^{t}Bu (**1^{IPr}**), prepared from previous literature,[31] was treated with bis(pinacolato)diboron (B_2pin_2) (1.1 equiv.) in *n*-pentane under an inert atmosphere of dinitrogen to form IPrCuB(pin) in situ, after which vinyl arene was added.[23] Gratifyingly, generation of IPrCu^{I}(β-borylbenzyl) complexes directly from **1^{IPr}** was possible, providing moderate to excellent yields. This synthetic route avoided isolation of more reactive, less stable IPrCu^{I}Bpin, and circumvented the decomposition observed when using the ICy ligand. Consistent with Sadighi's reported insertion rates of vinyl arenes into the Cu-Bpin bond, the more electron deficient substrates, such as para-fluorostyrene, reacted more quickly than more electron rich substrates, such as 4-*N*,*N*-dimethylaminostyrene. Some of the electron-deficient vinyl arenes that we employed did not yield the desired complexes, such as *p*-Cl and *p*-Br, which led to unproductive side reactions with no discernable product formed. The same was true in the case of *p*-cyanostyrene, findings consistent with previous literature.[23] Despite this, electron deficient Cu^{I}(β-borylbenzyl^{X}) complexes (X = acetoxy (AcO), methoxycarbonyl (CO_2Me), and trifluoromethyl (CF_3) substitution in the para position of the arene ring) were synthesized as tan powders in yields ranging from 44% to 67% (Scheme 2).

Scheme 2: Methods to synthesize spiroboralactonate-copper(I) complexes utilizing CO_2 and boron reductant.

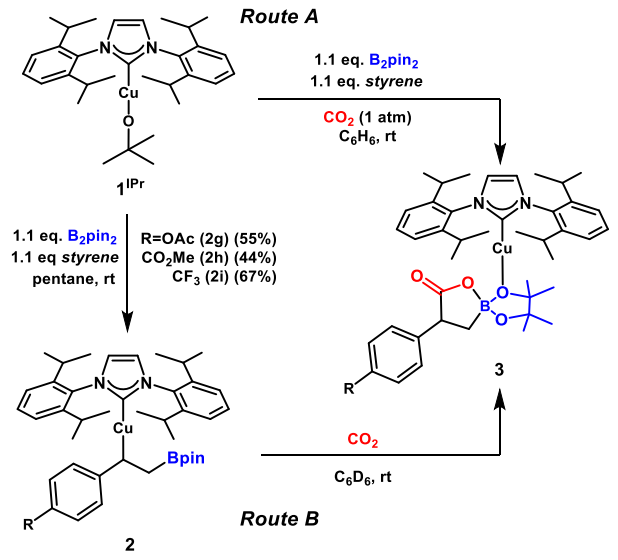

Characterization and reactivity of spiroboralactonate-copper(I) complexes: Inspired by reports indicating carboxylation occurs following insertion of alkynes into the Cu-E group (E=SiR_3, B(pin)),[15b,16b] we sought to validate a similar carboxylation pathway from Cu^I(β-borylbenzyl) complexes, **2**. We successfully synthesized a series of vinyl arene-derived boracarboxylated complexes through in situ generation of IPrCuBpin and the Cu^I(β-borylbenzyl) complexes under 1 atmosphere of CO_2 (Scheme 2, Route A). Complexes **3a**-**3f** were isolated after 16 hours as white powders in moderate to good yields (Table 1). Complexes bearing more electron deficient aryl substituents (i.e. **3g-3i**) were isolated after modifications were made to the stoichiometric conditions (Scheme 2, Method A and Table 1), including longer reaction time (48 hours) and inclusion of PPh_3 as an additive (*vide infra*).

Recognizing that carboxylation of vinyl arenes can occur through a *tert*-butoxide-catalyzed pathway unaided by copper,[32] the requisite Cu^I(β-borylbenzyl) complexes were isolated and purified following the protocol reported by Sadighi[23] (Scheme 2, Method B). Carboxylation was achieved by exposing benzene solutions of **2a-2i** with CO_2 gas (1 atm) at room temperature. Following the reaction, white solids were isolated and characterized as **3a-3i,** thus providing strong support for the role of copper in the carboxylation reaction. Interestingly, complex **2i** bearing the strongly electron deficient *p*-CF_3-benzyl moiety was carboxylated at a prohibitively slow rate such that only low yields of **3i** could be obtained for characterization purposes.

Table 1. Carboxylated copper(I) complexes isolated through stoichiometric boracarboxylation of vinyl arenes.[a]

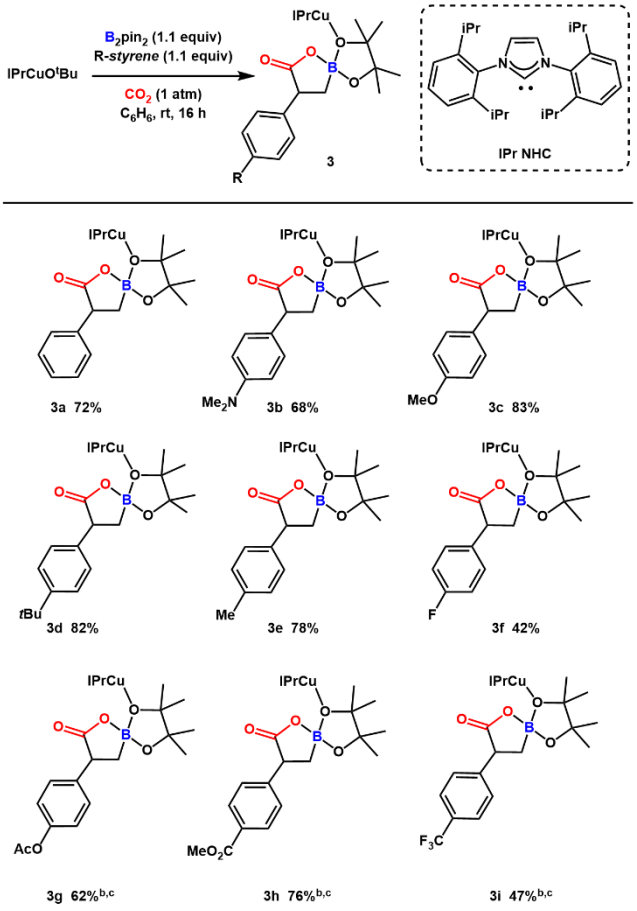

[a] Note: All spiroboralactonate complexes are represented as neutral for clarity. Formal charges are presumed to reside on the copper center (+1) and on the tetracoordinate boronate (-1). [b] 48 hr reaction time. [c] PPh_3 additive (1.0 equiv.).

Carboxylated complexes **3a-3i** were characterized using ^{1}H- and multi-nuclear NMR techniques as well as IR spectroscopy. The parent complex **3a**, for example, revealed a strong feature at 1711 cm^{-1} in the IR spectrum, indicative of the C=O stretch of a carbonyl functional group, likely resulting from inserted carbon dioxide. Comparison of ^{11}B NMR spectra of **2a** and **3a** showed a significant upfield shift of the B(pin) resonance from 34.7 ppm to 13.9 ppm, respectively, suggesting the formation of a four-coordinate boronate species rather than an open, κ^1-carboxylate complex.[33] This observation aligns well with ^{11}B NMR spectra reported for analogous boralactonates generated from alkyne substrates[15b] as well as other examples of non-coordinating arylspiroborate ligands.[34] The diastereotopic methylene group attached to boron also exhibits an shift upfield in both ^{1}H and ^{13}C NMR spectra, owing to increased electron density at boron upon formation of the spiroboralactonate ring.

The spiroboralactonate structure was confirmed upon collection of X-ray crystallographic data of **3a**. The molecular structure features an sp^3-hybridized boronate center, supported by the angles about the boron atom averaging 107° (Figure 1). This contrasts with crystallographic data of the unsubstituted boracarboxylic acid reported by Popp et al. previously,[19] from which it is clear from average bond angles of 120° that the boron is sp^2-hybridized. This assignment of an anionic tetracoordinate boron was also supported by the analogous copper complexes generated via the

boracarboxylation of alkynes.[15b] The nature of the copper-oxygen binding was confirmed to be through one of the pinacolate oxygens rather than the anticipated carboxylate oxygens. Once again, this type of binding is consistent with previously reported structures.

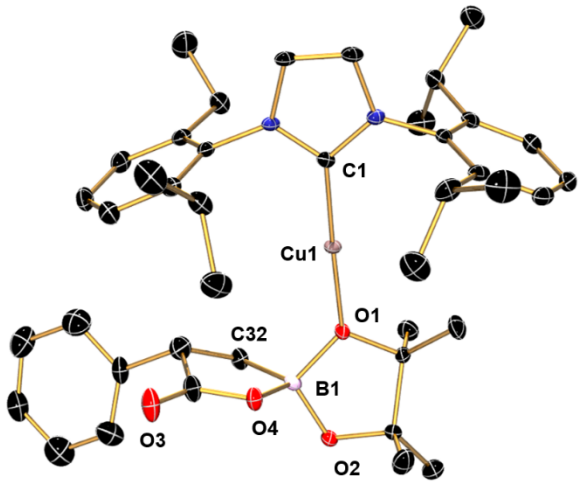

Figure 1. Molecular structure of **3a** with thermal ellipsoids set at 50% probability. H atoms have been omitted for clarity. Selected bond lengths (Å) and angles (deg): Cu1-C1, 1.910(3); Cu1-O1, 1.8568(14); O1-B1, 1.508(3); B1-O2, 1.4373; B1-O4 1.5313, B1-C32 1.618(3), O1-Cu1-C1 177.39(8); Cu1-O1-B1 129.31(12).

Variable-temperature (VT) ^{1}H NMR experiments were conducted in dichloromethane-d_2 to determine whether coordination of the copper center to the pinacol oxygen was maintained in solution. As the temperature is decreased from +25°C to -90°C, the spectrum of **3a** becomes more complex (Figure 2A). The singlet methyl resonances at 0.80 ppm representing two unique sets of methyl protons on the pinacol ring splits into four distinct singlet resonances, implying dynamic solution behavior. A similar effect was observed in VT ^{13}C NMR spectra, wherein inequivalent quaternary pinacol carbon resonances at -90 °C (83.4 and 77.0 ppm) collapse to a single resonance at +25 °C (81.3 ppm). Desymmetrization of the pinacol ring upon copper binding is further supported by 2D NMR experiments.[35] Geometry optimization of the solid-state structure for **3a** using DFT and subsequent natural bonding orbital (NBO) analysis revealed natural charges on the relevant oxygens (see Figure 1 for atom labels) that are consistent with copper binding at the more basic oxygen moiety. The natural charge on pinacol oxygens (O1: -0.89 | O2: -0.83) was noticeably larger, reflecting higher basicity, than the charges on carboxylate oxygens (O3: -0.65 | O4: -0.74). This is also consistent with natural charges calculated for the free spiroboralactonate anion (O1: -0.78 | O2: -0.78 | O3: -0.65 | O4: -0.74).

The dynamic behavior observed during ^{1}H VT-NMR studies of complex **3a** was further explored computationally. Close inspection of spiroboralactonate **3a** shows that two sets of diastereomeric structures are possible because the 5-membered borapinocolate ring can adopt two unique conformations. Thus, four ground-state structures for **3a** were identified from DFT geometry optimization using the SMD solvation model, with the most energetically feasible diastereomer pair shown in Figure 2B.[36] Interconversion between

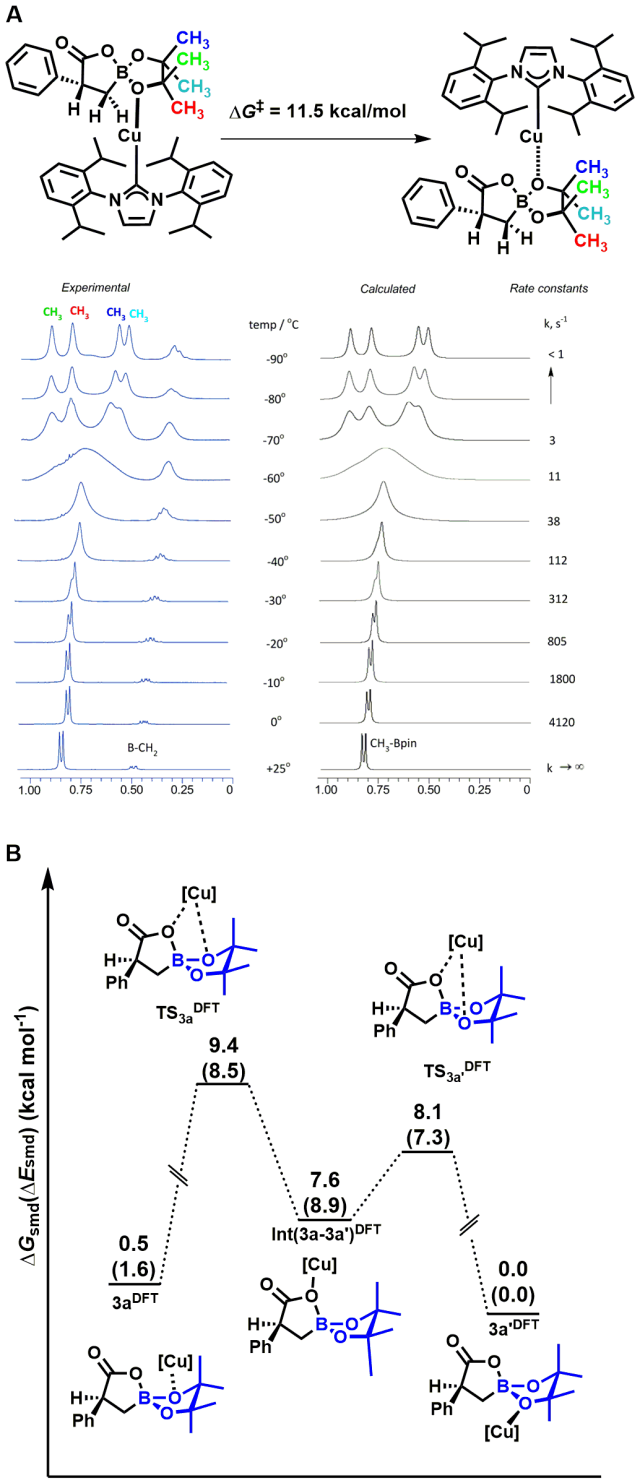

Figure 2. A) Experimental (left) and simulated (right) VT ^{1}H NMR spectrum demonstrating dynamic behavior in dichloromethane-d_2. Only the region containing the pinacolborane methyl resonances is shown for clarity. For full VT ^{1}H NMR spectra, see Figure S8. B) DFT-derived interconversion mechanism in dichloromethane (SMD solvation model), showing copper bound to each oxygen in the pinacol ring via a carboxylate-bound intermediate.

diastereomers **3a**^{DFT} and **3a´**^{DFT} proceeds by an inner-sphere mechanism via less-stable *k*^{1}-carboxylate intermediate **Int(3a-3a´)**$_{DFT}$. Comparison of experimental and computationally

predicted barriers (11.5 vs 9.4 kcal/mol, respectively) are in good agreement. Attempts to identify an outer-sphere ion-pair interconversion mechanism that bypasses **Int(3a-3a′)^{DFT}** using SMD solvent model were unsuccessful, yielding only high energy (> 40 kcal/mol) ion-pair intermediates. Ground state and transition state energies varied by less than 2 kcal/mol in both cases, which implies exchange occurs rapidly at room temperature and samples each isomeric geometry. Knowledge of such behavior could be consequential for future developments using spiroboronate salts for asymmetric catalysis utilizing a chiral anion.

Completion of the catalytic cycle is proposed to proceed through a salt metathesis reaction of spiroboralactonate copper salt with excess NaO^{t}Bu to produce a sodium spiroboralactonate salt and active ICyCuO^{t}Bu catalyst (Scheme 1, Step IV). In previous stoichiometric studies of alkyne boracarboxylation, an aggregate of the salt metathesis product stabilized by both tetrahydrofuran and lithium ion coordination was isolated and characterized.[15b] Similar treatment of **3a** with NaO^{t}Bu (1 equiv.) in THF for 30 minutes revealed formation of IPrCuO^{t}Bu via ^{1}H NMR characterization (Figure S9). Unfortunately, lack of solubility of the presumed metathesis product, sodium spiroboralactonate, prevented further isolation and characterization.[37]

^{1}H NMR spectroscopy was employed to monitor the salt metathesis reaction *in situ*. Given the low solubility of the spiroboralactonate product, the complex was dissolved in a mixture of 40%THF/benzene-d_6. Upon mixing **3a** and NaO^{t}Bu, resonances associated with the ethenyl protons of the NHC heterocycle of IPrCuO^{t}Bu were observed to increase over time with concomitant decrease of those associated with **3a** (Figure S10). Accompanying this change in the spectrum was the formation of a white solid, presumably sodium spiroboralactonate product. Further, upon addition of B_2pin_2 (1 equiv.) to the *in situ* NMR tube reaction mixture, IPrCuB(pin) increased with concomitant decrease of IPrCuO^{t}Bu based on observation of the ethenyl protons of the IPr heterocycle. Adding B_2pin_2 to a solution of **3a** excluding NaO^{t}Bu did not lead to the formation of IPrCuB(pin), suggesting that salt metathesis is necessary for catalytic turnover. This is consistent with conclusions from computational work by Lin showing the importance of the alkoxide base in promoting the salt metathesis step in the boracarboxylation of styrene.[26]

Kinetic analysis of carboxylation: Recent computational reports as well as experimental data obtained in our lab suggests that carboxylation serves as the turnover-limiting step of the catalytic boracarboxylation reaction (Scheme 1, Step III).[19,26,27,28] The electronic character of vinyl arene was important in terms of both yield and catalytic efficiency.[19] Specifically, higher yields were observed under ambient conditions with more electron-rich vinyl arenes whereas lower yields were observed for a limited group of moderately electron-deficient vinyl arenes (eg., *m*-fluorostyrene) under heating. This is in contrast to observations made for stoichiometric vinyl arene insertion into IPrCuB(pin), in which electron deficient vinyl arenes reacted more quickly.[23] Given the orthogonal reactivity of these two steps (Scheme 1, Step II and III), a better understanding of the carboxylation step is necessary.

The ethenyl protons of the IPr heterocycle on the Cu^I(β-borylbenzyl) complexes made the carboxylation reaction amenable to monitoring by ^{1}H NMR spectroscopy. Benzene-d_6 solutions of **2a-2i** were exposed to CO_2 (1 atm) in a J. Young NMR tube, and carboxylation was monitored to reaction completion. Over the course of the reaction, the growth of a single resonance for IPr ethenyl protons was observed downfield from that of the starting complex, consistent with formation of the carboxylate species **3a-3i** based on isolation/characterization studies described above. Reaction timecourses followed exponential behavior, and analysis of selected time courses demonstrated that the decay of starting material and concomitant increase of product occurred at similar rates (cf., Scheme S12). Carboxylation of Cu^I(β-borylbenzyl$^{p\text{-}NMe2}$) complex **2b** occurred in less than 10 minutes, whereas no appreciable carboxylation (<5% based on NMR integration) and some intractable decomposition was observed for Cu^I(β-borylbenzyl$^{p\text{-}CF3}$) complex **2i**.

Several pathways were considered for carboxylation of the Cu^I(β-borylbenzyl) complexes (Figure 3): the direct insertion pathway involving an interaction between copper and the carbon dioxide molecule during the transition state; and electrophilic substitution proceeding with no copper mediation, both S_E1 and S_E2. In order to elucidate the mechanism, a Hammett analysis using pseudo-first order rate constants (k_{2nd})[38] and the σ_p parameter was performed for complexes **2a-2h** (Figure 4). A negative rho (p) value would be expected for direct insertion or S_E2 carboxylation, assuming minimal pre-ionization of the Cu-C_{benzyl} bond at the transition state, due to reduction of negative charge at the benzylic carbon with electron-withdrawing para substituents. However, if initial ionization of the Cu-C_{benzyl} bond is required prior to CO_2 bond formation, as would be the case in an S_E1 mechanism, then a positive p value (indicating negative charge buildup) would be expected due to the enhanced stability the anionic benzylic carbon by the electron-withdrawing aryl ring.

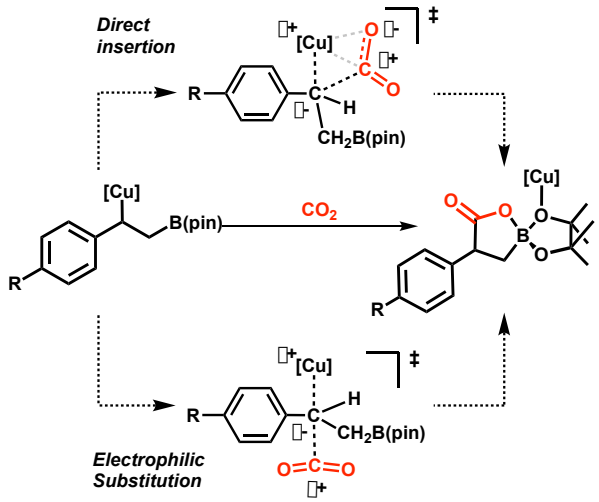

Figure 3. Potential pathways for the carboxylation of Cu^I(β-borylbenzyl) complexes.

The Hammett plot revealed a large ρ value (-1.61), which suggests positive charge buildup, or loss of negative charge, in the carboxylation transition state (Figure 4), which was inconsistent with an S_E1 mechanism.[32] The Hammett analysis, however, cannot distinguish between direct insertion and S_E2 pathways. Further, details related to the intimate interactions along the pathways are not available from experiment alone. Computational modeling became necessary to answer questions such as: does direct insertion of CO_2 proceed through Dewar-Chatt-Duncanson π-backbonding to CO_2 and formation

of a copper(III)-like intermediate/transition state, and does the boron moiety play a significant role in either pathway?

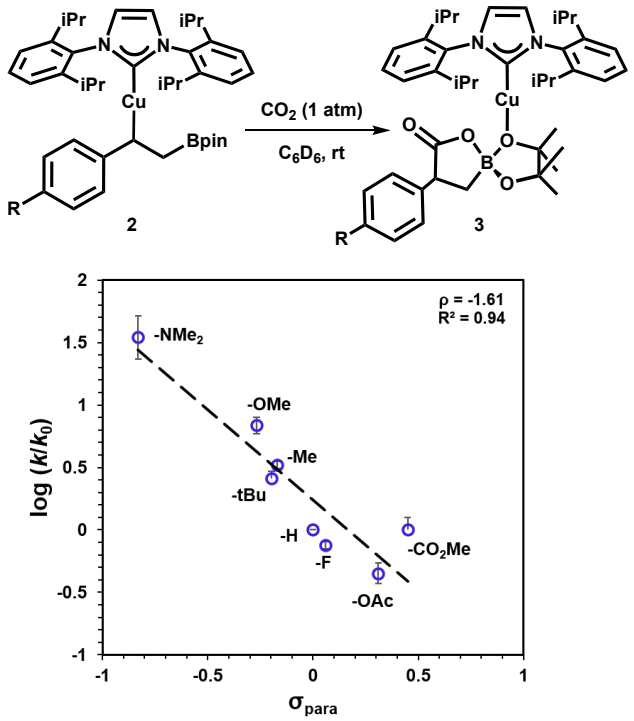

Figure 4. Hammett plot of relative rates of carboxylation of Cu^{I}(β-borylbenzyl) complexes **2a-2h**. The labels in the plot reflect the substitution in the 4-position of the aryl ring.

DFT was used to model the carboxylation of Cu^{I}(β-borylbenzyl) complexes. This serves to compliment the experimental data obtained here as well as bridge a gap in the existing computational literature on boracarboxylation of vinyl arenes.[39] Initial comparison of barriers resulting from Computational expense was reduced by replacing IPr and B(pin) with IMe ligand (IMe =1,3-bis(dimethyl)imidazol-2-ylidene) and B(eg) (eg = ethyleneglycato), which is a strategy used in other studies of related Cu^{I}-catalyzed transformations.[26,27,28,40] Para substituents of same or similar electronic character were used to mimic experimental complexes. In a recent publication, we reported that the S_E-like carboxylation pathways were disfavored relative to direct insertion (Figure 3).[28] Thus, following optimization of each Cu^{I}(β-borylbenzyl) model complex (denoted ***4a-i*** and corresponding to the experimental complex ***2a-i***), direct CO_2 insertion transition states for each complex were identified.[41,42,43,44] The SMD solvation-corrected relative Gibbs free energies of carboxylation ($\Delta\Delta G^{\ddagger}_{smd}$) were compared to σ_{para} as well as to experimentally derived $\Delta\Delta G^{\ddagger}$ values (Figure 5A). Attempts to identify a meta-stable CO_2 intermediate prior to **4a•TS** were unsuccessful, and IRC calculations validated the concerted conversion from Cu^{I}(β-borylbenzyl) to the carboxylation transition state **4a•TS** (Figure 5B).

DFT-calculated free energy changes were in reasonable agreement with experimental data (Figure 5A), with more electron-rich arenes (eg., -NH_2, **4b**, and -OMe, **4c**) exhibiting systemically lower barriers than electron-deficient arenes (eg., -CO_2H, **4h** and -CF_3, **4i)**. Calculated carboxylation barriers for the full IPrCu^{I}(β-borylbenzyl) complexes (**2a^{DFT}, 2b^{DFT}, 2i^{DFT}**) revealed a qualitatively similar electronic dependence. We also evaluated the S_E pathway for IMe and IPr ligated systems with trifluoromethyl and amino para-substituents, which showed essentially no electronic dependence on the barrier height (less than 1 kcal/mol) (see Table 2, below). In sum, these computational results strongly suggest that the experimentally observed carboxylation data is consistent with direct insertion as the kinetically favored pathway for IPr-ligated copper complexes.

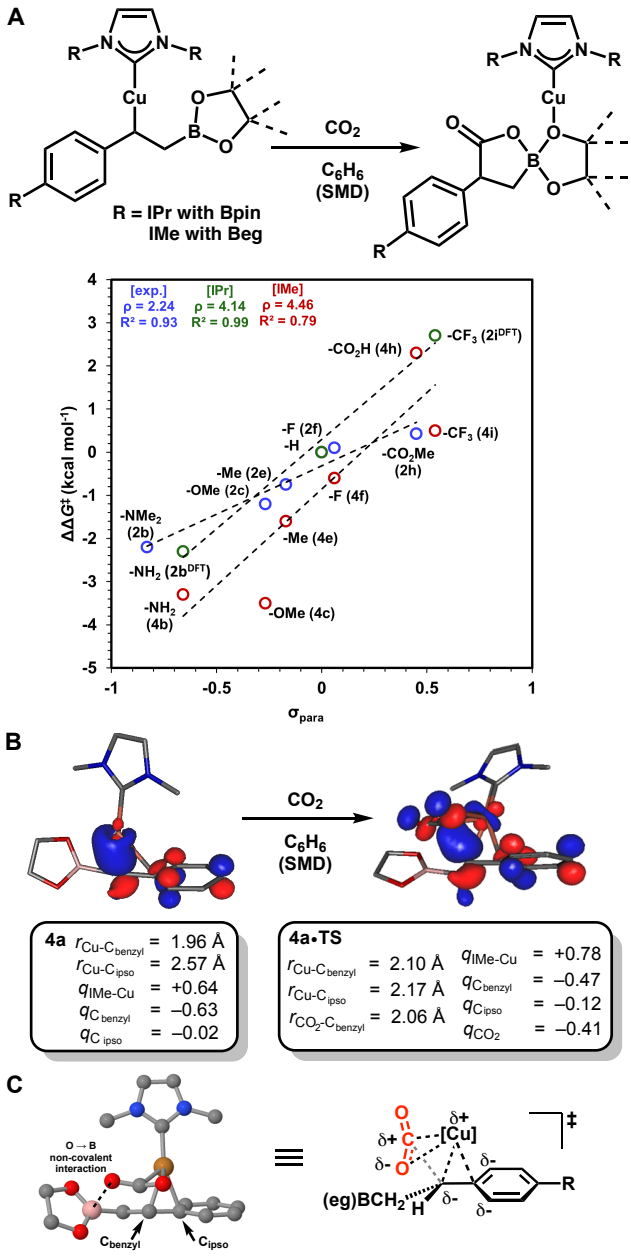

Figure 5. A) Comparison of experimental (IPr-ligated, blue) and computational (IPr-ligated, green and IMe-ligated, red) $\Delta\Delta G^{\ddagger}$ energies for the carboxylation of Cu^{I}(β-borylbenzyl) compounds. B) Rendering of the highest occupied molecular orbital (HOMO) for IMeCu(β-borylbenzyl) **4a** and direct insertion transition state **4a•TS**. Metrical parameters and natural charges (q) for relevant fragments obtained from NBO analysis. C) Ball-and-stick structure of direct insertion transition state **4a•TS** with cartoon depiction the key stereoelectronic interactions interactions at the transition state.

Visualization of **4a** (cf., Figure 5B) showed slight deviation from the idealized linear geometry expected in the IMe-Cu-C_{benzyl} bond angle, allowing a weak non-covalent interaction of the Cu center with neighboring C_{ipso} of the Ar ring. At transition state **4a•TS**, lengthening of Cu-C_{benzyl} (1.96 → 2.10 Å) with concomitant shortening of Cu-C_{ipso} (2.57 → 2.17 Å) bonds were noted. Similar metrical changes were observed for the other direct insertion carboxylation transition states. Notably, electron-rich benzyl complexes (eg., -NH_2, **4b**), that react fastest with CO_2, also featured the greatest asymmetry in the Cu-$C_{benzyl/ipso}$ bonds whereas electron-poor benzyl complexes (eg., -CF_3, **4i**), that react slowest with CO_2, feature similar Cu-$C_{benzyl/ipso}$ bond lengths (Table S3). We ascribe these systematic geometric changes to the increasing importance of benzyl anion stabilization in electron-deficient arenes, and consequently carboxylation barrier destabilization, through delocalization and multi-point copper coordination similar to that observed in π-benzyl complexes.[10e,45] Molecular orbital analysis of the HOMO of both **4a** and **4a·TS** supports this conclusion. The HOMO of **4a·TS** possesses significant benzyl and copper character. Coplanarity of the benzyl π-system allows delocalization of the HOMO across the aryl unit, which leads to significant electronic impacts upon arene ring substitution as reflected in the Hammett study.

Natural bond orbital (NBO) analysis of the electronically perturbed transition states was also performed to gain deeper insight into the direct insertion carboxylation pathway. Natural charges (q) were compared (Figure 5B and Table S3) to address specific sites of charge buildup and localization inferred from the experimental Hammett analysis. The combined natural charge of the C_{benzyl} and C_{ipso} (q_C) carbons and the extent of charge transfer to CO_2 at the transition state systematically decreased with increased electron withdrawing character of the para substituent. The IMe-Cu fragment natural charge becomes more positive at the transition state (cf., Figure 5B, Δq = +0.14) suggesting the possibility that the copper center is formally oxidized through π-backbonding to the incoming CO_2 electrophile. However, further MO and NBO investigations showed no significant copper-based orbital overlap with CO_2. Rather, increased charge buildup at the C_{ipso} carbon (Δq = −0.10) suggests that the copper center backdonates electron density to the aryl ring upon formation of a π-benzyl-like structure at the transition state.

The emerging stereoelectronic picture (Figure 5C) suggests that the aryl para-substituents impact the nucleophilicity of the benzylic carbon, thus the early (better nucleophile, lower barrier) vs. late (poorer nucleophile, higher barrier) nature of the transition state. Given this description of the direct insertion carboxylation transition state, we speculated that the boron moiety, being positioned inside the B-O van der Waals radii, may help further stabilize the early transition state through cooperative polarization of the C=O bond as we conceptually demonstrated recently.[28] All metrical and NBO parameters (eg., natural charge, boron valency, B-O orbital overlap), however, showed no correlation to the observed kinetic trend. This finding suggests that while boron (Bpin) may help orient CO_2 for insertion, the boronic ester utlized in this study is not sufficiently Lewis acidic to impart significant activation of CO_2 in the direct insertion transition state.

Additive influence in stoichiometric carboxylation of Cu^{I}(β-borylbenzyl) complexes: The use of Lewis basic additives in catalytic reactions is a common strategy to enhance reactivity, increase enantioselectivity, and expand methodology scope.[46] In our attempts to improve on scope limitations of the original boracarboxylation conditions,[19] we observed that the addition of PPh_3 to catalytic reactions led to enhanced reactivity of 4-trifluoromethylstyrene, allowing for isolation of the respective carboxylic acid in modest yields.[21] Given that the electron deficient *p*-CF_3 complex **2i** was not amenable to standard stoichiometric carboxylation nor to *in situ* NMR reaction monitoring, we suspected that PPh_3 may facilitate stoichiometric carboxylation as well. Thus, the reaction was repeated by introducing PPh_3 (1 equiv.) to a benzene-d_6 solution containing **2i**, which was subsequently monitored by ^{1}H NMR spectroscopy after addition of CO_2 gas. Indeed, product **3i**, identified by comparison to independently synthesized material (Scheme 2, Method A), was observed. The reaction was slow with a 6% yield of **3i** after the first 3 hours of the reaction. In contrast, no discernable quantity of **3i** was produced over several days when no PPh_3 was added. A further six-fold rate enhancement relative to PPh3 (1 equiv.) was observed when 1 equiv. of the more electron rich, sterically smaller PEt_3 was added to the carboxylation of **2i** (Figure S14-S15). Monitoring a benzene-d^6 solution of **2a** by ^{31}P NMR spectroscopy showed no new ^{31}P resonances in the presence or absence of CO_2 with 1.0 equivalent of phosphine additve, which is consistent with the formation of a meta-stable Cu^{I}–PPh_3 adduct intermediate prior to carboxylation.

This kinetic effect with phosphine additives has been observed in other Cu-catalyzed reactions; however, the mechanisms are not well understood.[47] Our stoichiometric model reaction offered an excellent opportunity to gain insight. Thus, we examined the kinetic impact of PPh_3 concentration over a range of 0.5-5.0 equivalents (Figure 6). The initial rate of carboxylation increases with a mild saturation dependence on PPh_3 concentration up to 3 equivalents. Given the lack of reactivity observed in stiochiometric studies discussed in the previous section, this perhaps indicates that an alternate carboxylation pathway is operative and outcompetes direct insertion of CO_2 into the electron deficient Cu^{I}(β-borylbenzyl) complex. Addition of PPh_3 at higher concentration (5 equiv.) led to diminished initial reaction rate with no appreciable side products detected. The impact of PPh_3 concentration on the reaction rate for carboxylation of eletron rich *p*-tBu complex **2d** was then examined (Figure 5B). No rate acceleration was observed,

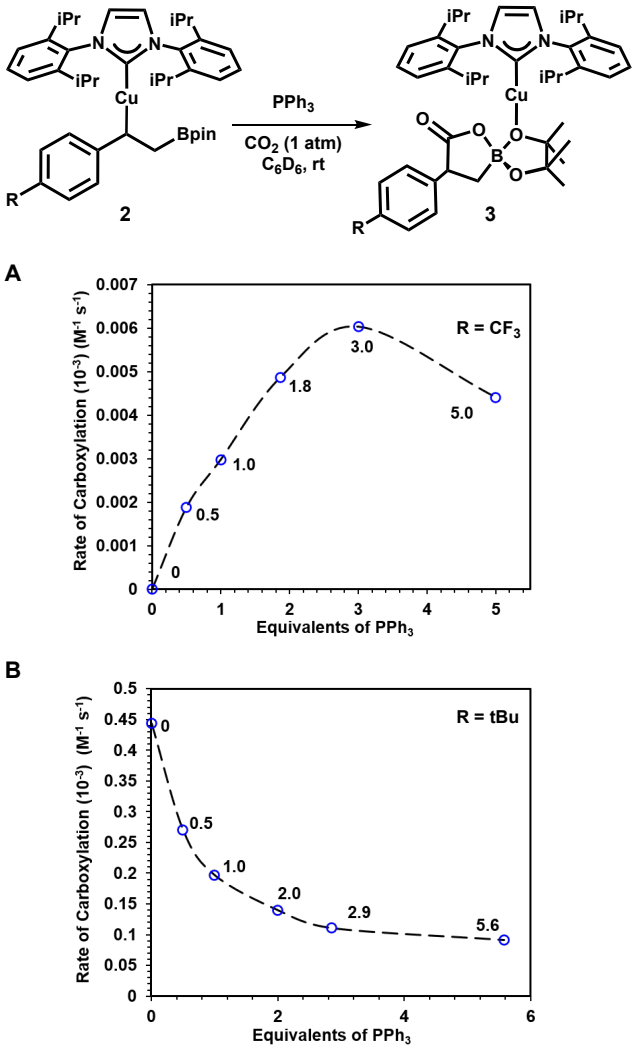

Figure 6. Rates of carboxylation for A) *p*-CF_3 complex **2i** with varying amounts of PPh_3 and B) tBu complex **2d** with varying amounts of PPh_3.

but rather, PPh_3 significantly inhibits the reaction. The addition of multiple equivalents of PPh_3 (up to 5.6 equiv.) resulted in an overall 15-fold decrease in the initial rate of carboxylation as compared to the reaction containing no additive. Interestingly, the inhibition of **2d** carboxylation proceeds at a rate that is 2-fold faster than the enhancement of **2i** carboxylation. This disparity in the observed rate profiles implies that PPh_3 acts directly on the Cu^I(β-borylbenzyl) complex and either accelerates or inhibits caboxylation depending on the electronic characteristics of the benzyl moiety. We reasoned that prior reversible coordination of PPh_3 at the copper center would shut down the direct insertion carboxylation pathway (Figure 7). At the same time, the ionization of the benzyl ligand may also become more favorable due to the congestion caused by PPh_3. This would explain why a benzyl derivative bearing an anion stablizing withdrawing group on the arene would lead to carboxylation product, presumably through an S_E-like transition state. This proposed additive effect contrasts mechanistic findings in alkene hydrocarboxylation in which PPh_3 is thought to sequester promiscuous copper species during catalysis,[21] and therefore, appears to be a unique addition to additive effect mechanisms.

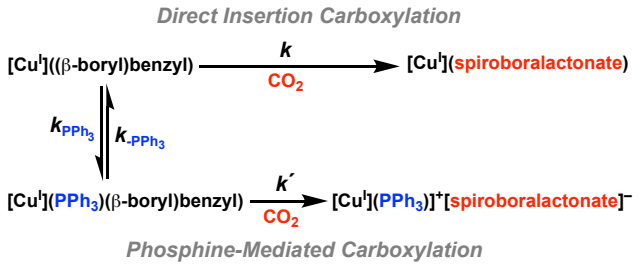

Figure 7. Proposed competitve pathways for carboxylation with PPh_3 additive.

We initiated computational studies by examining the ligation of PPh_3 to the full IPrCu(β-borylbenzyl) **2a**^{DFT}. In the PPh_3-mediated pathway, the additive was predicted to generate a three-coordinate copper(I)-phosphine species following ligation to **2a**. A meta-stable ground state intermediate (**2a•PPh$_3$**) was identified, destabilized on the free energy surface relative to **2a** by 9.3 kcal/mol (Figure S28). The intermediate features significant bending out of plane of IMe to accommodate the PMe_3. The intermediate has a Cu–P bond length of 2.9 Å, which, although longer than those reported for tri-coordinate copper(I)phosphine complexes (2.26 Å on average),[49] is within the sum of Van der Waals radii for the two atoms (3.2 Å).[51] Unfortunately subsequent calculations of the carboxylation pathway were generally unsuccessful due to poor convergence to optimized minima and saddlepoints.

We turned to the truncated IMe ligand model system as well as smaller PMe_3 was used in calculations to elucidate the full proposed competitive carboxylation mechanism. A structurally similar meta-stable ground state intermediate (**4a•PMe$_3$**) was identified (Figure S28), and destabilized on the free energy surface relative to **4a** by 6.1 kcal/mol (Figure 8). Counterpoise corrections for the intermediate were calculated to be approx. 2 kcal/mol (Table S4). As expected, the sterically less encumbered intermediate possesses a significantly shorter Cu-P bond (2.36 Å). Relaxed potential energy surface scans of PMe_3 coordination to **4a** revealed a flat energy surface in which the approximate transition state and intermediate **4a•PMe$_3$** were essentially isoenergetic. Subsequently, an early transition state (**4a•PMe$_3^{TS}$**) was as identified, showing little deviation in the copper complex geometry relative to **4a** as well as a long Cu–P bond distance (3.15 Å). The free energy barrier is less than 8 kcal/mol, suggesting that more sterically bulky systems, such as the experimental system, should be able to access **2a•PPh$_3$**. The DFT model energetics are consistent with our inability to observe such a complex by NMR spectroscopy.

We next investigated the ability of CO_2 to undergo direct insertion into trigonal intermediate **4a•PMe$_3$**. All attempts to locate a transition state in which CO_2 inserts into the sterically congested copper center were unsuccessful. Alternative pathways in which carboxylation proceeds through backside electrophilic substitution at the benzyl carbon (ie., S_E-like addition) were then considered.

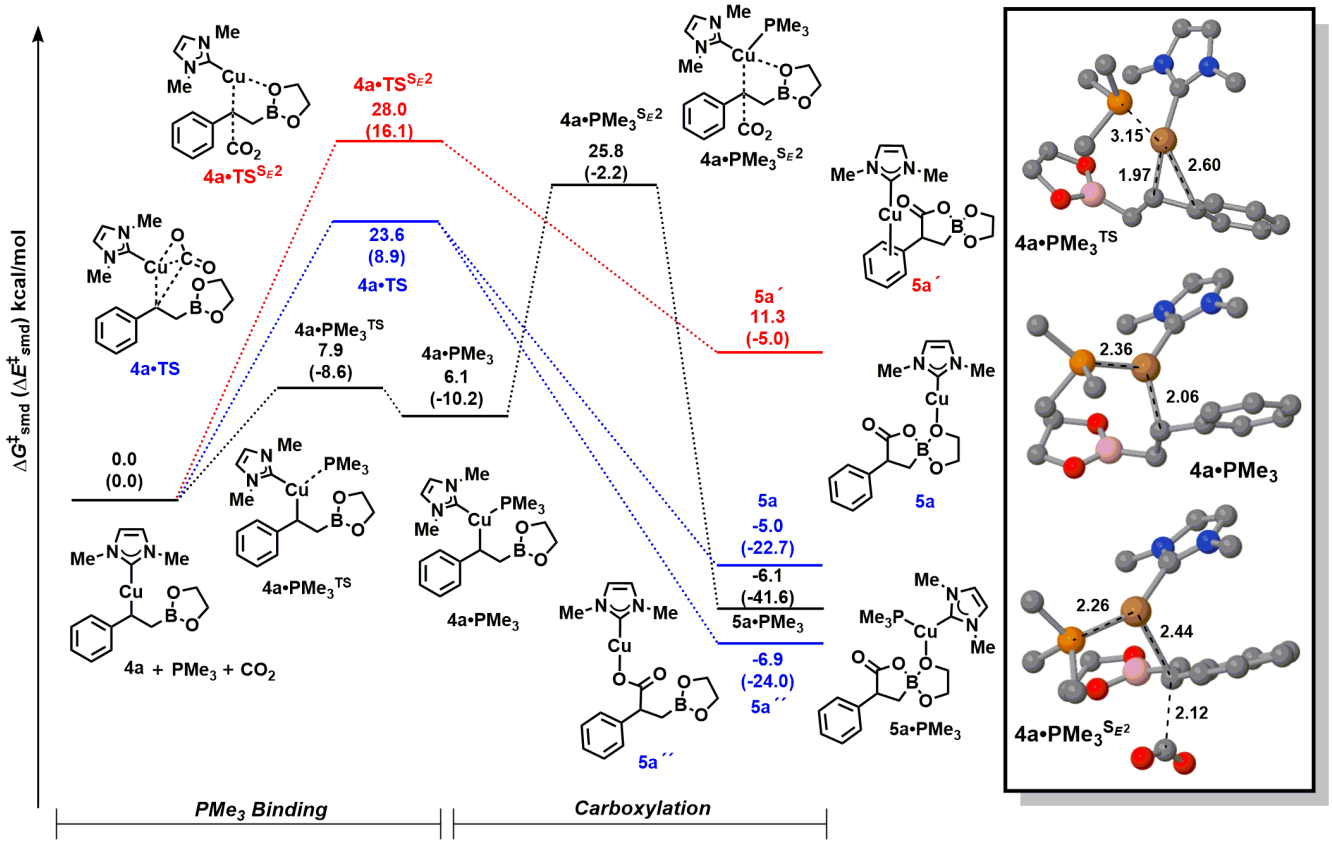

Figure 8. Reaction coordinates for carboxylation via: 1) direct insertion (blue), 2) unassisted S_E2 (red) and 3) PMe_3-assisted S_E2 (black). Each spiroboralactonate structure is depicted as neutral for clarity; the formal charges in these complexes would be drawn at the copper (+1) and the tetracoordinate boron (-1) atoms.

Electrophilic (S_E1) addition through initial full ionization of the Cu-benzyl bond was considered but deemed highly unlikely due to our dynamics analysis of **3a** that showed ion-pair formation between IPrCu cation and spiroborolactonate to be energetically prohibitive. Electrophilic (S_E2) addition was next considered. Multiple transition states were identified depending on the orientation of the Beg moiety. The most stabilized transition state (**4a•PMe$_3$-S_E**) resulted from Beg positioned close to the Cu center, providing an anchor as depicted in Figure 8. A transition state with similar geometry was previously identified for unassisted electrophilic substitution.[28] The free energy of activation for the PMe_3-assisted pathway (**4a•PMe$_3$-S_E**) was over 2 kcal/mol more favorable than the unassisted pathway (ie., **4a•PMe$_3$-S_E** and **4a•TS^{S_E}**, respectively); however, the direct addition barrier was still more stable by over 2 kcal/mol. These results are consistent with the diverging reactivity observed in PPh_3 concentration dependence studies in which inhibition by PPh_3 is expected due to the favorability of direct insertion carboxylation.

After establishing a viable pathway for phosphine-mediated carboxylation, we performed calculations on the IPrCu system with PMe_3 ligand. The PMe_3 ligand is a reasonable steric and electronic model for the PEt_3 additive experiment described above (cf., Figure S14). An intermediate (**2a•PMe$_3$**) was identified and was structurally similar to those identified for the minimalist and full models (cf., Figure 28). The phosphine-assisted electrophilic carboxylation transition state (**2a•PMe$_3$-S_E**, $\Delta G^{\ddagger}$ = 30.7) was notably higher in energy than the unassisted transition state (**2a•TS^{S_E}**, $\Delta G^{\ddagger}$ = 24.3) by 6.4 kcal/mol (Table 2).

Comparison of the metrics and natural charges of electrophilic substitution ground state and transition state structures revealed substantial differences (Figure 9). Consistent with expectation, PMe_3 binding, forming **4a•PMe$_3$**, resulted in a longer Cu-C_{benzyl} bond (Δr = 0.1 Å) relative to **4a**. This effect was more apparent when comparing the electrophilic substitution transition states in which the Cu-C_{benzyl} bond increases by 0.26 Å, leading to the more accessible, energetically stabilized transition state **4a•PMe$_3$-S_E**. The unassisted transition state **4a•TS^{S_E}** features a similar Cu-C_{ipso} interaction observed in the direct insertion transition state **4a•TS**; in fact, **4a•TS^{S_E}** has a quite short Cu-C_{ipso} bond length of 2.05 Å. This ipso-interaction is not structurally feasible in the PMe_3-assisted pathway and likely is the major reason why the additive

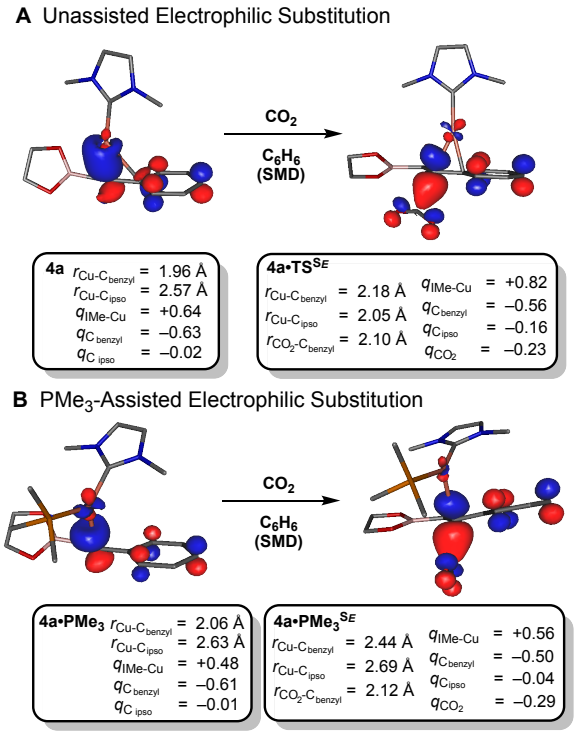

Figure 9. Renderings of the highest occupied molecular orbital (HOMO) for electrophilic substitution pathways as well as metrical parameters and natural charges (q) for relevant fragments obtained from NBO analysis.

leads to a stabilized carboxylation barrier. Visualization of the respective HOMO of unassisted and PMe_3-assisted transition states shows reduced copper character and significant benzyl anion character, as would be anticipated for an S_E1-like transition state in the latter case (Figure 9). PMe_3 plays a key role in stabilizing the cationic copper center at this transition state as indicated by the significantly reduced natural charge (q = +0.56) at the IMe-Cu fragment (cf., q = +0.82 at **4a•TS^{SE}**), as well as leading to greater charge transfer from the benzyl anion to the CO_2 moiety.

Evaluation of electrophilic carboxylation of electronically perturbed NHCCu^{I}(β-borylbenzyl^{X}) complexes (NHC = IPr, **2x,** and IMe, **4x**, for **x** = -H (**a**) -NH_2 (**b**) and -CF_3 (**i**)) by DFT shed further light on the role of PMe_3 (Table 2). In the unassisted pathway, minimal electronic effects were observed with free energy barriers separated by less than 1.5 kcal/mol. This reflects differing electronic contributions at the transition state arising from increasing π-benzyl-like character due to the Cu-C_{ipso} interaction. In the PMe_3-assisted carboxylation pathway, electronic effects were more important, with the most electron-deficient complex **2i** being lowest in energy and the most electron rich complex **2b** being highest in energy ($\Delta G^{\ddagger}$ = 30.4 vs. 30.7 kcal/mol, respectively). The former transition state also features the longest Cu-C_{benzyl} bond (2.78 Å) and least negative charge on C_{benzyl} atom. These results are consistent with observations made above that support an S_E1-like description of the phosphine-assisted pathway. NHC ligand size and phosphine additive size clearly impact the magnitude of the respective transition states. However, it is important to recall that PEt_3 additive does indeed enhance the rate of **2i** carboxylation experimentally whereas in the absense of additive no carboxylation is observed, suggesting that absolute energetic comparisons with current DFT models should be viewed cautiously.

Table 2. Computationally derived Gibbs free energy barriers associated with electrophilic carboxylation and corresponding key metrical and natural charge (q) parameters for the PMe_3-assisted transition state.

p-Ar Subs.	$\Delta G^{\ddagger a}$ **2|4•TS^{SE}**	$\Delta G^{\ddagger a}$ **2|4•PMe$_3$S$_E$** [a]	Cu-C_{benzyl} (Å) **2|4•PMe$_3$S$_E$**	C_{benzyl} q **2|4•PMe$_3$S$_E$**
CF_3	25.0 | 27.3	30.4 | 23.9	2.78 | 2.46	-0.46 | -0.48
H	24.3 | 28.0	30.7 | 25.8	2.53 | 2.44	-0.52 | -0.50
NH_2	25.7 | 27.5	34.5 | 26.9	2.34 | 2.33	-0.55 | -0.53

[a] Relative to the sum of **2*x*** *or* **4*x***, CO_2 (and PMe_3) in kcal/mol.

CONCLUSIONS

In this work, we have presented an experimental and computational mechanistic study of key steps proposed in the copper(I)-catalyzed boracarboxylation of vinyl arenes. Preparation of a library of unique IPrCu^{I}-spiroboralactonate salts was achieved through stoichiometric reactions from both IPrCuO^{t}Bu and IPrCu^{I}(β-borylbenzyl^{X}) complexes. Multinuclear NMR techniques as well as X-ray crystallography were used to characterize the solution behavior and solid-state structure of the carboxylated copper complexes.

Kinetic studies provided insight into the mechanisms by which carboxylation is possible. A strong dependence was observed on the electronic character of the arene, which is due to the impact on the benzylic carbon poised for nucleophilic attack. An experimental Hammett analysis corroborated prior computational evidence that direct insertion was the energetically preferred pathway by which carbon dioxide is incorporated under standard boracarboxylation conditions. Further analysis of NBO-derived natural charges for the ground- and transition-state structures associated with carboxylation indicated that copper interacts with the ipso carbon of the arene ring in a manner similar to that observed in π-benzyl complexes. This interaction was critical in explaining the experimental Hammett data.

A second feasible S_E-like mechanism was identified when carboxylation was performed in the presence of electron-rich additive, PPh_3 or PEt_3. We showed computational evidence of the formation of a tri-coordinate copper-PPh_3 intermediate that facilitates weakening of the Cu-C_{benzyl} bond, allowing for more facile backside attack on CO_2. Our results suggest that alternative pathways are likely accessible and a more nuanced approach to methodology development, with consideration of reaction conditions as well catalyst and/or substrate steric/electronic characteristics, will be necessary to fully understand the kinetic preferences of involved carboxylation pathways.

EXPERIMENTAL SECTION

General Information: All air- and moisture-sensitive manipulations were performed under a dry atmosphere of nitrogen using Schlenk line techniques and under a nitrogen atmosphere in an Mbraun glovebox. Solvents used were purchased from Fisher and were further dried through a Glass Contour Solvent Purification System and stored over 4Å molecular sieves. Dichloromethane was further dried with CaH_2, vacuum transferred, and stored over 4Å molecular sieves. Liquid reagents were degassed via freeze/pump/thaw method, and solids are dried under vacuum

prior to transfer to the glovebox. Dry carbon dioxide was passed through drying column containing desiccant prior to use.

^{1}H, ^{13}C, ^{19}F, and ^{11}B NMR spectra were recorded using Agilent 400 MHz, JEOL 400 MHz, and Varian INOVA 600 MHz NMR spectrometers. Deuterated benzene (C_6D_6) and dichloromethane (CD_2Cl_2) were distilled from sodium metal and calcium hydride, respectively, and stored in the glovebox. IPrHCl,[50] IPrCuCl,[51] IPrCuOtBu,[31] and IPrCu-(β-borylbenzyl) complexes **2a-2f** were prepared following reported literature procedures.[23] PPh_3 and PEt_3 were purchased from standard chemical suppliers, transferred to an inert atmosphere glovebox and used as received.

Synthesis of Complexes 2g-2i: Compounds were prepared from the following procedure modified from literature:[23] Under an atmosphere of N_2, 1 equiv. of IPrCuO^{t}Bu (100 mg, 0.19 mmol) was combined with 1.1 equiv. of B_2pin_2 (54 mg, 0.21 mmol) in 5 mL of *n*-pentane. After stirring at ambient temperature for 10 minutes, 1.1 equiv. of the appropriate styrene (0.21 mmol) was added. The reaction was stirred for 1 hour, after which time the solid was collected on a fine porosity glass frit through vacuum filtration and was washed with *n*-pentane (2x).

2g - IPrCu^I(CH(^{pOCOMe}Ph)CH$_2$Bpin). Yield: 78 mg (0.11 mmol, 55%). ^1H NMR (400 MHz, benzene-d_6) δ 7.92 (d, J = 8.2 Hz, 2H), 7.26 (t, J = 7.8 Hz, 2H), 7.03 (ddd, J = 7.7, 6.4, 1.5 Hz, 4H), 6.72 – 6.67 (d, J =8.3 Hz, 2H), 6.17 (s, 2H), 3.71 (s, 3H), 2.77 (t, J = 7.3 Hz, 1H), 2.41 (h, J = 7.0 Hz, 4H), 1.57 (t, J = 6.6 Hz, 2H), 1.23 (dd, J = 14.3, 6.8 Hz, 12H), 1.03 (dd, J = 7.0, 2.7 Hz, 12H), 0.96 (s, 12H). ^{11}B NMR (128 MHz, benzene-d_6) δ 35.27 ppm. ^{13}C NMR (101 MHz, benzene-d_6) δ 185.37 ($C_{carbene}$), 169.38, 156.95, 145.61, 143.22, 135.31, 130.42, 124.59, 124.23, 122.00, 120.45, 81.82, 29.70, 28.97, 25.15, 24.94, 23.73, 23.67, 20.99, 16.01(br).

2h - IPrCu^I(CH($^{p\text{-}CO2Me}$Ph)CH$_2$Bpin): Yield: 62 mg (0.08 mmol, 44%). ^1H NMR (400 MHz, benzene-d_6) δ 7.29 (t, J = 7.8 Hz, 2H), 7.14 (dd, J = 7.7, 3.1 Hz, 4H), 6.81 (d, J = 8.6 Hz, 2H), 6.72 (d, J = 8.5 Hz, 2H), 6.20 (s, 2H), 2.51 (dp, J = 13.7, 7.2 Hz, 5H), 1.85 (s, 3H), 1.61 (d, J = 5.4 Hz, 2H), 1.32 (dd, J = 9.9, 6.9 Hz, 12H), 1.09 (dd, J = 6.9, 1.8 Hz, 12H), 0.98 (s, 12H). ^{13}C NMR (151 MHz, benzene-d_6) δ 184.77, 168.11, 164.89, 145.49, 135.13, 130.57, 130.02, 124.19, 122.99, 122.18, 117.96, 82.03, 28.93, 25.12, 25.09, 24.90, 24.86, 23.74, 23.70. ^{11}B NMR (128 Hz, benzene-d_6) δ 34.70 ppm.

**2i - IPrCu^I(CH($^{p\text{-}CF3}$Ph)CH$_2$Bpin): ***50 mg of IPrCuOtBu was used in this reaction. Yield: 48 mg (0.06 mmol, 67%). ^1H NMR (400 MHz, benzene-d_6) δ 7.24 (t, J = 7.8 Hz, 2H), 7.19 (d, J = 8.2 Hz, 2H), 7.06 – 7.00 (m, 4H), 6.68 – 6.63 (m, 2H), 6.17 (s, 2H), 2.65 (t, J = 7.5 Hz, 1H), 2.42 (dp, J = 8.6, 6.8 Hz, 4H), 1.57 (d, J = 2.0 Hz, 1H), 1.55 (s, 1H), 1.25 (d, J = 6.9 Hz, 6H), 1.21 (d, J = 6.9 Hz, 6H), 1.04 (dd, J = 6.9, 1.6 Hz, 12H), 0.97 (s, 12H). ^{13}C NMR: (101 MHz, benzene-d_6) δ 184.8, 163.4, 145.5, 135.1, 130.5, 124.7, 124.2, 124.1, 123.3, 122.1, 82.0, 32.2, 28.9, 25.0, 24.9, 23.7, 23.6, 14.7. ^{11}B NMR (128 Hz, benzene-d_6): 33.43 ppm. ^{19}F NMR (376 MHz, benzene-d_6): δ -59.85 ppm.

Synthesis of 3a-3f: Under an atmosphere of N_2, a Schlenk flask equipped with a magnetic stir bar was charged with 1 equiv. of IPrCuO^{t}Bu (100 mg, 0.190 mmol) and 1.1 equiv. B_2pin_2 (54 mg, 0.21 mmol) in 10 mL of benzene. 1.1 equiv. of the appropriate styrene (0.21 mmol) was added to the reaction vessel. Using Schlenk line techniques, the reaction underwent 3 freeze/pump/thaw cycles to remove the headspace as well as any dissolved nitrogen gas. After evacuation, 1 atmosphere of dry CO_2 gas was added, and the reaction stirred at ambient temperature for 16 hours. The resulting suspensions underwent 2 additional freeze/pump/thaw cycles before returning to the glovebox. The solvent was removed *in vacuo*, and the resulting compounds were washed with *n*-pentane and collected on a fine porosity glass frit as white solids.

3a - IPrCu^I((CO$_2$)CHPhCH$_2$Bpin)): Yield: 99 mg (0.14 mmol, 72%). ^1H NMR (400 MHz, dichloromethane-d_2) δ (ppm) 7.50 (t, J = 7.8 Hz, 2H), 7.35 (d, J = 6.4 Hz, 4H), 7.24 (d, J = 5.0 Hz, 2H), 7.20 (d, J = 7.4 Hz, 1H), 7.12 – 7.06 (m, 2H), 2.78 (t, J = 8.8 Hz, 1H), 2.56 (p, J = 7.0 Hz, 4H), 1.27 (dd, J = 26.6, 6.8 Hz, 21H), 0.85 (d, J = 7.0 Hz, 10H), 0.55 – 0.45 (m, 2H). ^{13}C NMR (101 MHz, dichloromethane-d_2) δ 146.2, 134.9, 131.3, 128.7, 128.3, 125.9, 125.0, 124.9, 124.3, 81. 3, 54.4, 54.2, 54.0, 53.8, 53.6, 49.7, 29.4, 25.4, 25.3, 25.0, 24.3, 24.3. ^{11}B NMR (128 MHz, dichloromethane-d_2) δ (ppm) 13.9. IR ν (KBr pellet, CH_2Cl_2): 1711 cm^{-1}. Colorless single crystals suitable for X-ray analysis were obtained by slow diffusion of *n*-pentane into a concentration dichloromethane solution at -35°C.

3b - IPrCu^I((CO$_2$)CH(^{pNMe2}Ph)CH$_2$Bpin)): Yield: 99 mg (0.13 mmol, 68%). ^1H NMR (400 MHz, dichloromethane-d_2) δ 7.52 (t, J = 7.8 Hz, 2H), 7.36 (d, J = 7.7 Hz, 4H), 7.26 (s, 2H), 6.95 (d, J = 8.4 Hz, 2H), 6.68 – 6.61 (m, 2H), 2.89 (s, 6H), 2.68 (t, J = 8.8 Hz, 1H), 2.57 (hept, J = 7.0 Hz, 4H), 1.31 (d, J = 6.9 Hz, 12H), 1.24 (d, J = 6.9 Hz, 12H), 0.85 (d, J = 6.0 Hz, 12H), 0.46 (d, J = 8.8 Hz, 2H). ^{13}C NMR (101 MHz, dichloromethane-d_2) δ 181.4, 179.2, 149.6, 146.2, 134.9, 133.5, 131.3, 128.9, 124.9, 124.3, 113.2, 81.2, 48.6, 41.4, 30.3, 29.3, 25.5, 25.3, 25.0, 24.3. ^{11}B NMR (128 MHz, dichloromethane-d_2): δ (ppm) 13.73. IR ν (KBr pellet, dichloromethane film): 1699 cm^{-1} (C=O).

3c - IPrCu^I((CO$_2$)CH(^{pOCH3}Ph)CH$_2$Bpin)): Yield: 120 mg (0.16 mmol, 83%). ^1H NMR (400 MHz, dichloromethane-d_2) δ 7.50 (t, J = 7.8 Hz, 2H), 7.35 (d, J = 7.7 Hz, 4H), 7.24 (s, 2H), 7.02 (d, J = 8.3 Hz, 2H), 6.76 (d, J = 8.5 Hz, 2H), 3.77 (s, 3H), 2.72 (t, J = 8.8 Hz, 1H), 2.56 (p, J = 6.9 Hz, 4H), 1.30 (d, J = 6.9 Hz, 12H), 1.24 (d, J = 6.9 Hz, 12H), 0.85 (d, J = 6.9 Hz, 12H), 0.47 (d, J = 8.9 Hz, 2H). ^{13}C NMR (101 MHz, dichloromethane-d_2) δ 181.0, 179.2, 158.1, 146.2, 137.1, 134.9, 131.3, 129.4, 128.9, 124.9, 124.2, 113.6, 81.3, 55.7, 48.7, 30.3, 29.3, 25.4, 25.3, 25.0, 24.3. ^{11}B NMR (400 MHz, dichloromethane-d_2) δ (ppm) 14.32. IR ν (KBr pellet, dichloromethane film): 1709 cm^{-1} (C=O).

3d - IPrCu^I((CO$_2$)CH(^{ptBu}Ph)CH$_2$Bpin)): Yield: 122 mg (0.16 mmol, 82%). ^1H NMR (400 MHz, benzene-d_6 / dichloromethane-d_2) δ 7.26 (td, *J* = 7.8, 1.4 Hz, 2H), 7.14 (s, 4H), 7.12 (s, 2H), 7.10 (t, *J* = 7.5 Hz, 2H), 6.50 (d, *J* = 1.6 Hz, 2H), 3.01 (t, *J* = 8.6 Hz, 1H), 2.45 – 2.29 (m, 4H), 1.27 – 1.14 (m, 21H), 1.08 – 0.96 (m, 12H), 0.91 – 0.83 (m, 12H), 0.78 (dd, *J* = 14.4, 7.8 Hz, 1H), 0.68 – 0.60 (m, 1H). ^{13}C NMR (101 MHz, benzene-d_6 / dichloromethane-d_2) δ 180.0, 147.6, 145.3, 141.8, 134.2, 130.6, 127.8, 127.7, 124.5, 80.7, 48.8, 33.9, 31.1, 28.5, 24.9, 24.8, 24.4, 23.5. ^{11}B NMR (128 MHz, benzene-d_6 / dichloromethane-d_2) δ 17.55. IR ν (KBr pellet, dichloromethane film): 1707 cm^{-1} (C=O).

3e - IPrCu^I((CO$_2$)CH(^{pMe}Ph)CH$_2$Bpin)). Yield: 110 mg (0.15 mmol, 78%). ^1H NMR (400 MHz, dichloromethane-d_2) δ 7.50 (t, *J* = 7.8 Hz, 2H), 7.35 (d, *J* = 7.7 Hz, 4H), 7.24 (s, 2H), 7.06 – 6.93 (m, 4H), 2.73 (t, *J* = 8.8 Hz, 1H), 2.56 (hept, *J* = 7.2 Hz, 4H), 2.29 (s, 3H), 1.27 (dd, *J* = 25.9, 6.9 Hz, 24H), 0.85 (d, *J* = 7.1 Hz, 12H), 0.48 (d, *J* = 8.9 Hz, 2H). ^{13}C NMR (101 MHz, dichloromethane-d_2) δ 180.9, 179.2, 146.2, 142.0, 134.9, 131.3, 128.9, 128.9, 128.4, 124.9, 124.3, 81.3, 49.2, 29.3, 25.4, 25.3, 25.0, 24.3, 21.3. ^{11}B NMR (128 MHz, dichloromethane-d_2) δ 13.85. IR ν (KBr pellet, dichloromethane film): 1717 cm^{-1} (C=O).

3f - IPrCu^I((CO$_2$)CH(^{pF}Ph)CH$_2$Bpin)). Yield: 59 mg (0.08 mmol, 42%). ^1H NMR (400 MHz, dichloromethane-d_2) δ 7.48 (t, *J* = 7.8 Hz, 2H), 7.34 (s, 4H), 7.24 (s, 2H), 7.11 (dd, *J* = 8.4, 5.6 Hz, 2H), 6.91 (t, *J* = 8.8 Hz, 2H), 2.78 (t, *J* = 9.0 Hz, 1H), 2.55 (p, *J* = 7.0 Hz, 4H), 1.29 (d, *J* = 6.9 Hz, 12H), 1.23 (d, *J* = 6.8 Hz, 12H), 0.85 (d, *J* = 7.0 Hz, 12H), 0.49 (q, *J* = 7.1, 5.8 Hz, 2H). ^{13}C NMR (101 MHz, dichloromethane-d_2) δ 162.8, 160.4, 146.2, 140.6, 134.9, 131.3, 130.1, 130.0, 124.9, 124.3, 114.8, 114.6, 81.4, 48.7, 29.3, 25.4, 25.3, 25.0, 24.3. The resonance associated with the methylene carbon is not detectable, most likely due to its proximity to quadrapolar boron. ^{11}B NMR (128 MHz, dichloromethane-d_2) δ 14.55 ppm. ^{19}F NMR (376 MHz, dichloromethane-d_2) δ -119.44 ppm. IR ν (KBr, dichloromethane film): 1709.3 cm^{-1} (C=O).

Complexes **3g-3i** were synthesized similarly to the general procedure. However, the addition of PPh_3 was necessary in order to achieve synthetically reasonable reaction times.

3g - IPrCu^{I}((CO$_2$)CH(^{pOCOMe}Ph)CH$_2$Bpin)). Yield: 92 mg (0.12 mmol, 62%). ^{1}H NMR (400 MHz, benzene-d$_6$/dichloromethane-d$_2$) δ 7.71 (t, *J* = 7.7 Hz, 2H), 7.57 (t, *J* = 7.2 Hz, 4H), 7.51 (d, *J* = 8.3 Hz, 2H), 7.24 (s, 2H), 3.20 (t, *J* = 8.7 Hz, 1H), 2.80 (dt, *J* = 13.6, 6.8 Hz, 4H), 2.42 (s, 3H), 1.59 (d, *J* = 6.8 Hz, 12H), 1.47 (d, *J* = 6.8 Hz, 12H), 1.17 (d, *J* = 6.0 Hz, 12H), 0.90 (d, *J* = 8.7 Hz, 2H). ^{13}C NMR (101 MHz, benzene-d$_6$/dichloromethane-d$_2$) δ 180.11 (C$_{CO2}$), 178.90 (C$_{carbene}$), 169.74(C$_{OCOMe}$), 149.01, 145.85, 142.23, 134.60, 131.09, 129.31, 124.65, 123.79, 121.13, 81.09, 53.52, 48.74, 29.05, 25.20, 25.11, 24.86, 24.00, 21.09. ^{11}B NMR (128 MHz, benzene-d$_6$/dichloromethane-d$_2$) δ 11.23 ppm. IR ν (KBr pellet, dichloromethane film) 1710 cm^{-1} (C=O, carboxylate), 1762 cm^{-1} (C=O, ester).

3h - IPrCu^{I}((CO$_2$)CH(^{pCOOMe}Ph)CH$_2$Bpin)). Yield: 111 mg (0.14 mmol, 74%). ^{1}H NMR (600 MHz, dichloromethane-*d*$_2$) δ 7.89 (dd, *J* = 8.1, 5.9 Hz, 2H), 7.47 (t, *J* = 7.8 Hz, 2H), 7.34 (t, *J* = 9.0 Hz, 4H), 7.25 (s, 2H), 7.22 (d, *J* = 8.0 Hz, 2H), 3.88 (s, 3H), 2.84 (t, *J* = 9.0 Hz, 1H), 2.56 (h, *J* = 6.8 Hz, 4H), 1.30 (d, *J* = 10.9 Hz, 12H), 1.24 (d, *J* = 6.8 Hz, 12H), 0.86 (d, *J* = 12.3 Hz, 12H), 0.55 (qd, *J* = 14.1, 8.9 Hz, 2H). ^{13}C NMR (151 MHz, dichloromethane-*d*$_2$) δ 179.73 (C$_{CO2}$), 179.08(C$_{carbene}$), 167.65 (C$_{CO2Me}$), 150.36, 146.22, 134.92, 131.31, 129.53, 128.66, 127.97, 124.84, 124.31, 81.47, 52.26, 49.58, 29.35, 25.40, 25.30, 25.05, 24.33, 24.29. ^{11}B NMR (128 MHz, dichloromethane-d$_2$) δ 12.20 ppm. IR ν (KBr pellet, tetrahydrofuran film) 1719 cm^{-1} (overlapping).

3i - IPrCu^{I}((CO$_2$)CH(^{pCF3}Ph)CH$_2$Bpin)). Yield: 71 mg (0.09 mmol, 47%). ^{1}H NMR (400 MHz, dichloromethane-d$_2$) δ 7.51 – 7.39 (m, 4H), 7.35 – 7.24 (m, 6H), 7.23 (s, 2H), 2.80 (t, J = 9.0 Hz, 1H), 2.52 (hept, J = 7.1 Hz, 4H), 1.26 (d, J = 6.9 Hz, 12H), 1.21 (d, J = 6.9 Hz, 12H), 0.82 (d, J = 8.2 Hz, 12H), 0.56 – 0.45 (m, 2H). ^{13}C NMR (101 MHz, dichloromethane-d$_2$) δ 179.69, 148.99, 146.20, 134.85, 131.24, 128.93, 125.09, 124.93, 124.79, 124.28, 81.44, 54.27, 49.26, 29.29, 25.32, 25.22, 25.05, 24.22. The methylene carbon is not visible in ^{13}C NMR as it is broad due to the quadrupolar nature of the adjacent boron. ^{19}F NMR (376 MHz, dichloromethane-d2) δ -62.34. ^{11}B NMR (128 MHz, dichloromethane-d$_2$) δ 12.50. IR ν (KBr pellet, dichloromethane film) 1708 cm^{-1} (C=O).

Carboxylation Kinetics: The following procedure was used in performing kinetic experiments for the carboxylation of Cu^{I}(β-borylbenzyl) complexes. Under a N$_2$ glovebox atmosphere, 5 mg of each Cu^{I}(β-borylbenzyl) complex (**2a-2i**) was dissolved in C$_6$D$_6$ and combined with mesitylene as an internal standard (0.1 M in C$_6$D$_6$) to produce a 10 mM sample. The sample was transferred to a J. Young NMR tube and was removed from the glovebox. Using Schlenk techniques, the sample was freeze/pump/thawed 2 times. The sample was then cooled to -20°C (1:3 NaCl/ice bath), and the evacuated headspace was filled with 1 atm of dry CO$_2$. The tube was resealed and kept frozen until loading into the NMR instrument. Spectra were then collected at consistent intervals for the duration of the reaction using the array feature in VNMRJ software.

X-Ray Crystallography: Single crystals suitable for X-Ray diffraction were coated with polybutene oil (Sigma-Aldrich), placed on a MiTeGen nylon loop, and then quickly mounted on the goniometer head of a Bruker AXS D8 Venture fix-chi X-ray diffractometer equipped with a Triumph monochromator, a Mo Kα radiation source (I=0.71073 Å), and a PHOTON 100 CMOS detector. Samples were cooled to 100 K with an Oxford Cryostream 700 system and optically aligned. Three sets of 12 frames each were collected using the omega scan method with a 10 second exposure time. Integration of these frames followed by reflection indexing and least-squares refinement produced a crystal orientation matrix for the monoclinic crystal lattice that was used for the structural analysis. The APEX3 software program (version 2016.9-0)[52] was used for diffractometer control, preliminary frame scans, indexing, orientation matrix calculations, least-squares refinement of cell parameters, and the data collection. The frames were integrated with the Bruker SAINT software package using a narrow-frame algorithm. Data were corrected for absorption effects using the multi-scan method (SADABS). The structure was solved by direct methods and difference Fourier analysis using the programs provided by SHELXL-2014/7.2.[53] Further collection and refinement information is reported in the supporting information.

Computational Methods: All calculations were performed using the Gaussian 16 package.[54] For ground state and transition state geometry optimizations with IMe-ligated copper complexes, the M06 functional and Pople-style basis sets 6-311+G(d) (Cu) and 6-311G(d) (all other atoms) were used.[55,56] For ground state and transition state geometry optimizations with IPr-ligated copper complexes, B3LYP with Grimme's D3 dispersion and Pople-style basis sets 6-311+G(d) (Cu) and 6-311G(d) (all other atoms) were used.[57,58] Comparison of IMe- and IPr-ligated copper complexes with M06 functional and the basis set described above were possible in a limited number of cases. Additional computational method benchmarking data is available in the Supporting Information. Frequency calculations at the same level of theory in each case were performed to validate stationary points, with zero imaginary frequencies reflecting a ground state minimum and one imaginary frequency representing a transition state saddle point. Transition states were further validated through intrinsic reaction coordinate (IRC) calculations.[59] Single-point self-consistent reaction field calculations (SCRF) were also performed to identify solvent effects using the SMD model.[60] Benzene was used in solvent calculations to reflect the experimental conditions in the kinetic studies. JMol was used to generate optimized molecular structures.[61]

ASSOCIATED CONTENT

Supporting Information

Full complex characterization including crystallographic data for **3a** (CCDC-2002370) (CIF), kinetics data, and computational results. This material is available free of charge via the Internet at http://pubs.acs.org.

AUTHOR INFORMATION

Corresponding Author

* Brian V. Popp: Brian.Popp@mail.wvu.edu

Funding Sources

This research was supported by a National Science Foundation (NSF) Career Award (CHE-1752986). The NMR spectrometer, X-ray diffractometer, and high-performance computing system (Thorny Flat) used in this research were supported by the NSF Major Research Instrumentation (MRI) program (CHE-1228336, CHE-1336071, OAC-1726534).

Notes

The authors declare no competing financial interests.

ACKNOWLEDGMENT

We would like to thank the National Science Foundation and West Virginia University Department of Chemistry and High-Performance Computing Center for their generous support of this research.

REFERENCES

(1) (a) Artz, J.; Müller, T. E.; Thenert, K. Sustainable Conversion of Carbon Dioxide: An Integrated Review of Catalysis and Life Cycle Assessment. *Chem. Rev.* **2018**, *118*, 434-504. (b) Liu, Q.; Wu, L.; Jackstell, R.; Beller, M. Using Carbon Dioxide as a Building Block in

Organic Synthesis. *Nat. Commun.* **2015**, *6*, 5933-5948. (c) Aresta, M.; Dibenedetto, A.; Angelini, A. Catalysis for the Valorization of Exhaust Carbon: from CO_2 to Chemicals, Materials, and Fuels. Technological Use of CO_2. *Chem. Rev.* **2014**, *114*, 1709-1742. (d) Tsuji, Y.; Fujihara, T. Carbon Dioxide as a Carbon Source in Organic Transformations: Carbon-Carbon Bond Forming Reactions by Transition-Metal Catalysts. *Chem. Commun.* **2012**, *48*, 9956-9964. (e) Peters, M.; Köhler, B.; Kuckshinrichs, W.; Leitner, W.; Markewitz, P.; Müller, T. E. Chemical Technologies for Exploiting and Recycling Carbon Dioxide into the Value Chain. *ChemSusChem* **2011**, *4*, 1216-1240. (f) Sakakura, T.; Choi, J.; Yasuda, H. Transformation of Carbon Dioxide. *Chem. Rev.* **2007**, *107*, 2365-2387.

(2) Meesen, J. Urea Synthesis. *Chem. Ing. Tech.* **2014**, *86(12)*, 2180-2189.

(3) Behr, A. *Carbon Dioxide Activation by Metal Complexes.* VCH: Weinheim, **1988.**

(4) Burkhart, M. D.; Hazari, N.; Tway, C. L.; Zeitler, E. L. Opportunities and Challenges for Catalysis in Carbon Dioxide Utilization. *ACS Catal.* **2019**, *9,* 7937-7956.

(5) Jessop, P. G.; Joó, F.; Tai, C. C. Recent Advances in the Hydrogenation of Carbon Dioxide. *Coord. Chem. Rev.* **2004**, *248*, 2425-2442.

(6) Solmi, M. V.; Schmitz, M.; Leitner, W. Chapter 6: CO_2 as a Building Block for the Catalytic Synthesis of Carboxylic Acids, in *Studies in Surface Science and Catalysis*; Elsevier: Amsterdam, **2019**.

(7) Tortajada, A.; Julía-Hernández, F.; Börjesson, M.; Moragas, T.; Martin, R. Transition-Metal-Catalyzed Carboxylation Reactions with Carbon Dioxide. *Angew. Chem. Int. Ed.* **2018**, *57*, 15948-15982

(8) *Carboxylic Acid Compound Classes: Pharmaceuticals and Agrochemicals.* Wiley-VCH: Weinheim, **2016.**

(9) Maag, H. *Prodrugs of Carboxylic Acids;* Springer: New York, **2007**.

(10) For selected reviews on transition metal-facilitated carboxylation chemistry, see (a) Li, H. R.; He, L. N. Construction of C-Cu Bond: A Useful Strategy in CO_2 Conversion. *Organometallics* **2020**, *39*, 1461-1475. (b) Zhang, L.; Li, Z.; Takimoto, M.; Hou, Z. Carboxylation Reactions with Carbon Dioxide Using N-Heterocyclic Carbene-Copper Catalysts. *Chem. Rec.* **2019**, *19*, 1-20. (c) Yang, Y.; Lee, J. Toward Ideal Carbon Dioxide Functionalization. *Chem. Sci.* **2019**, *10*, 3905-3926. (d) Cokoja, M.; Bruckmeier, C.; Rieger, B.; Herrmann, W. A.; Kühn, F. E. Transformation of Carbon Dioxide with Homogeneous Transition-Metal Catalysts: A Molecular Solution to a Global Challenge? *Angew. Chem. Int. Ed.* **2011**, *50*, 8510-8537. (e) Obst, M.; Pavlovic, L.; Hopmann, K. H. Carbon-Carbon Bonds with CO_2: Insights from Computational Studies. *J. Organomet. Chem.* **2018**, *864*, 115-127.

(11) For select examples of C-B bond carboxylation, see: (a) Kuge, K.; Luo, Y.; Fujita, Y.; Mori, Y.; Onodera, G.; Kimura, M. Copper-Catalyzed Stereodefined Construction of Acrylic Acid Derivatives from Terminal Alkynes via CO_2 Insertion. *Org. Lett.* **2017**, *19*, 854-857. (b) Juhl, M.; Laursen, S. L. R.; Huang, Y.; Nielsen, D. U.; Daasbjerg, K.; Skrydstrup, T. Copper-Catalyzed Carboxylation of Hydroborated Disubstituted Alkenes and Terminal Alkynes with Cesium Fluoride. *ACS Catal.* **2017**, *7*, 1392-1396. (c) Duong, H. A.; Huleatt, P. B.; Tan, Q. W.; Shuying, E. L. Regioselective Copper-Catalyzed Carboxylation of Allylboronates with Carbon Dioxide. *Org. Lett.* **2013**, *15*, 4034-4037. (d) Ohishi, T.; Nishiura, M.; Hou, Z. Carboxylation of Organoboronic Esters Catalyzed by N-Heterocyclic Carbene Copper(I) Complexes. *Angew. Chem. Int. Ed.* **2008**, *47*, 5792-5795; and references therein. (12) For select examples of C-Sn bond carboxylation, see: (a)Feng, X.; Sun, A.; Zhang, S.; Yu, X.; Bao, Palladium-Catalyzed Carboxylative Coupling of Benzyl Chlorides with Allyltributylstannane: Remarkable Effect of Palladium Nanoparticles. *Org. Lett.* **2013**, *15*, 108-111. (b) Franks, R. J.; Nicholas, K. M. Palladium-Catalyzed Carboxylative Coupling of Allylstannanes and Allyl Halides. *Organometallics*. **2000**, *19*, 1458-1460. (c) Shi, M.; Nicholas, K. M. Palladium-Catalyzed Carboxylation of Allyl Stannanes. *J. Am. Chem. Soc.* **1997**, *119*, 5057-5058.

(13) For selected examples of C-H bond carboxylation utilizing CO_2, see: (a) Takimoto, M.; Gholap, S. S.; Hou, Z. Alkylative Carboxylation of Ynamides and Allenamides with Functionalized Alkylzinc Halides and Carbon Dioxide by a Copper Catalyst. *Chem. Eur. J.* **2019**, *25*, 8363-8370. (b) Sahoo, B.; Bellotti, P.; Juliá-Hernández, F.; Meng, Q.; Crespi, S.; König, B.; Martin, R. Site-Selective, Remote sp^3 C-H Carboxylation Enabled by the Merger of Photoredox and Nickel Catalysis. *Chem. Eur. J.* **2019**, *25*, 9001-9005. (c) Ishida, N.; Masuda, Y.; Imamura, Y.; Yamazaki, K.; Murakami, M. Carboxylation of Benzylic and Aliphatic C-H Bonds with CO_2 Induced by Light/Ketone/Nickel. *J. Am. Chem. Soc.* **2019**, *141*, 19611-19615. (d) Saini, S.; Singh, H.; Prajapati, P. K.; Sinha, A. K.; Jain, S. L. Nickel/Nickel Oxide in Combination with a Photoredox Catalyst for the Reductive Carboxylation of Unsaturated Hydrocarbons with CO_2. *ACS Sustainable Chem. Eng.* **2019**, *7*, 11313-11322. (e) Hong, J.; Li, M.; Zhang, J.; Sun, B.; Mo, F. C-H Carboxylation with Carbon Dioxide. *ChemSusChem* **2019**, *12*, 6-39.

(14) For selected examples of C-X bond carboxylation utilizing CO_2, see: (a) Wang, H.; Gao, Y.; Zhou, C.; Li, G. Visible-Light-Driven Reductive Carboarylation of Styrenes with CO_2 and Aryl Halides. *J. Am. Chem. Soc.* **2020**, *142,* 8122-8129. (b) Charboneau, D. J.; Brudvig, G. W.; Hazari, N.; Lant, H. M. C.; Saydjari, A. K. Development of an Improved System for the Carboxylation of Aryl Halides through Mechanistic Studies. *ACS Catal.* **2019**, *9*, 3228-3241. (c) Yan, S.; Wu, D.; Ye, J.; Gong, L.; Zeng, X.; Ran, C.; Gui, Y; Li, J.; Yu, D. Copper-Catalyzed Carboxylation of C-F Bonds with CO_2. *ACS Catal.* **2019**, *9*, 6987-6992. (d) Bhunia, S. K.; Das, P.; Nandi, S.; Jana, R. Carboxylation of Aryl Triflates with CO_2 Merging Palladium and Visible-Light-Photoredox Catalysts. *Org. Lett.* **2019**, *21*, 4632-4637. (e) Ma, C.; Zhao, C.; Xu, X.; Li, Z.; Wang, X.; Zhang, K.; Mei, T. Nickel-Catalyzed Carboxylation of Aryl and Heteroaryl Fluorosulfates Using Carbon Dioxide. *Org. Lett.* **2019**, *21*, 2464-2467.

(15) (a) Li, Z.; Zhang, L.; Nishiura, M.; Luo, G.; Hou, Z. CO_2 Activation by Lewis Pairs Generated Under Copper Catalysis Enables Difunctionalization of Imines. *J. Am. Chem. Soc.* **2020***,142, 4,* 1966-1974. (b) Zhang, L.; Cheng, J.; Carry, B.; Hou, Z. Catalytic Boracarboxylation of Alkynes with Diborane and Carbon Dioxide by an N-Heterocyclic Carbene Copper Catalyst. *J. Am. Chem. Soc.* **2012**, *134*, 14314-14317.

(16) (a) Tani, Y.; Fujihara, T.; Tsuji, Y. Copper-Catalyzed Regiodivergent Silacarboxylation of Allenes with Carbon Dioxide and a Silylborane. *J. Am. Chem. Soc.* **2014**, *136*, 17706-17709. (b) Fujihara, T.; Tani, Y.; Semba, K.; Terao, J.; Tsuji, Y. Copper-Catalyzed Silacarboxylation of Internal Alkynes by Employing Carbon Dioxide and Silaboranes. *Angew. Chem. Int. Ed.* **2012**, *51,* 11487-11490.

(17) (a) Miao, B.; Li, S.; Li, G.; Ma, S. Cyclic *Anti*-Azacarboxylation of 2-Alkynylanilines with Carbon Dioxide. *Org. Lett.* **2016**, *18*, 2556-2559. (b) Li, S.; Ma, S. Quadri-Synergetic Effect for Highly Effective Carbon Dioxide Fixation and Its Application to Indoloquinolone. *Adv. Synth. Catal.* **2012**, *354*, 2387-2394.

(18) There is one report of phosphonocarboxylation of alkenes that does not require a transition metal catalyst. Fu, Q.; Bo, Z. Y.; Ye, J. H.; Ju, T.; Huang, H.; Liao, L. L.; Yu, D. G. Transition Metal-Free Phosphonocarboxylation of Alkenes with Carbon Dioxide via Visible-Light Photoredox Catalysis. *Nature Commun.* **2019**, *10*, 1-9.

(19) (a) Fiorito, D.; Liu, Y.; Besnard, C.; Mazet, C. Direct Access to Chiral Secondary Amides by Copper-Catalyzed Borylative Carboxamidation of Vinylarenes with Isocyanates. *J. Am. Chem. Soc.* **2020**, *142*, 623-632. (b) Su, Z.; Feng, Y.; Zou, R.; Qiu, X.; Wang, J.; Tao, C. Copper-Catalyzed Borylamidation of Vinyl Arenes with Isocyanates. *Chem. Commun.* **2020**, *56*, 7438-7468. (c) Wu, N. Y.; Xu, X. H.; Qing, F. L. Copper-Catalyzed Regioselective Borylfluoromethylation of Alkenes. *ACS Catal.* **2019**, *9*, 5726-5731. (d) Chen, B; Cao, P.; Liao, Y.; Wang, M; Laio, J. Enantioselective Copper-Catalyzed Methylboration of Alkenes. *Org. Lett.* **2018**, *20,* 1346-1349. (e) Logan, K. M.; Sardini, S. R.; White, S. D.; Brown, M. K. Nickel-Catalyzed Stereoselective Arylboration of Unactivated Alkenes. *J. Am. Chem. Soc.* **2018**, *140*, 159-162. (f) He, S. L.; Wang, B.; Lu, X.; Gong, T. J.; Yang, Y. N.; Wang, X. X.; Wang, Y.; Xiao, B.; Fu, Y. Copper-Catalyzed

Reagent-Controlled Regioselective Cyanoborylation of Vinyl Arenes. *Org. Lett.* **2018**, *20*, 5208-5212. (g) Cheng, Y.; Mück-Lichtenfeld, C.; Studer, A. Transition Metal-Free 1,2-Carboboration of Unactivated Alkenes. *J. Am. Chem. Soc.* **2018**, *140*, 6221-6225. (h) Kim, N.; Han, J. T.; Ryu, D. H.; Yun, J. Copper-Catalyzed Asymmetric Borylallylation of Vinyl Arenes. *Org. Lett.* **2017**, *19*, 6144-6147. (i) Huang, Y.; Smith, K. B.; Brown, M. K. Copper-Catalyzed Borylacylation of Activated Alkenes with Acid Chlorides. *Angew. Chem. Int. Ed.* **2017**, *56*, 13314-13318.

(20) Butcher, T. W.; McClain, E. J.; Hamilton, T. G.; Perrone, T. M.; Kroner, K. M.; Donohoe, G. C.; Akhmedov, N. G.; Petersen, J. L.; Popp, B. V. Regioselective Copper-Catalyzed Boracarboxylation of Vinyl Arenes. *Org. Lett.* **2016**, *18*, 6428-6431.

(21) Perrone, T. M.; Gregory, A. S.; Knowlden, S. W.; Ziemer, N. R.; Alsulami, R. N.; Petersen, J. L.; Popp, B. V. Beneficial Effect of a Secondary Ligand on the Catalytic Difunctionalization of Vinyl Arenes with Boron and CO_2. *ChemCatChem* **2019**, *11*, 5814-5820.

(22) Laitar, D. S.; Müller, P.; Sadighi, J. P. Efficient Homogeneous Catalysis in the reduction of CO_2 to CO. *J. Am. Chem. Soc.* **2005**, *127*, 17196-17197.

(23) Laitar, D. S.; Tsui, E. Y.; Sadighi, J. P. Copper(I) β-Boroalkyls from Alkene Insertion: Isolation and Rearrangement. *Organometallics*. **2006**, *25*, 2405-2408.

(24) Mankad, N. P.; Gray, T. C.; Laitar, D. S.; Sadighi, J. P. Synthesis, Structure, and CO_2 Reactivity of a Two-Coordinate (Carbene)copper(I) Methyl Complex. *Organometallics* **2004**, *23*, 1191-1193.

(25) Bhattacharyya, K. X.; Akana, J. A.; Laitar, D. S.; Berlin, J. M.; Sadighi, J. P. Carbon-Carbon Bond Formation on Reaction of a Copper(I) Stannyl Complex with Carbon Dioxide. *Organometallics* **2008**, *27*, 2682-2684.

(26) Lin, S.; Lin, Z. DFT Studies on the Mechanism of Copper-Catalyzed Boracarboxylation of Alkene with CO_2 and Diboron. *Organometallics* **2019**, *38*, 2, 240-247.

(27) (a) Lv, X.; Wu, Y. B.; Lu, G. Computational Exploration of Ligand Effects in Copper-Catalyzed Boracarboxylation of Styrene with CO_2. *Catal. Sci. Technol.* **2017**, *7*,5049-5054. (b) García-López, D.; Pavlovix, L.; Hopmann, K. H. To Bind or Not to Bind: Mechanistic Insights into C-CO_2 Bond Formation with Late Transition Metals. *Organometallics* **2020,** *39,* 1339-1347.

(28) Baughman, N. N.; Popp, B. V. Evidence of Boron Assistance for CO_2 Activation during Copper-Catalyzed Boracarboxylation of Vinyl Arenes: A Synthetic Model for Cooperative Fixation of CO_2. *Comment. Inorg. Chem*. **2020**, *40*, 159-175.

(29) Laitar, D. S.; Tsui, E. Y.; Sadighi, J. P. Catalytic Diboration of Aldehydes via Insertion into the Copper-Boron Bond. *J. Am. Chem. Soc.* **2006**, *128*, 11036-11037.

(30) Herron, J. R.; Russo, V.; Valente, E. J.; Ball, Z. T. Catalytic Organocopper Chemistry from Organosiloxane Reagents. *Chem. Eur. J.* **2009**, *15*, 8713-8716.

(31) Mankad, N. P.; Laitar, D. S.; Sadighi, J. P. Synthesis, Structure, and Alkyne Reactivity of a Dimeric (Carbene)copper(I) Hydride. *Organometallics*. **2004**, *23*, 3369-3371.

(32) Grigg, R. D.; Rigoli, J. W.; Van Hoveln, R.; Neale, S.; Schomaker, J. M. Beyond Benzyl Grignards: Facile Generation of Benzyl Carbanions from Styrenes. *Chem. Eur. J.* **2012**, *18*, 9391-9396.

(33) Heřmánek, S. ^{11}B NMR Spectra of Boranes, Main-Group Heteroboranes, and Substituted Derivatives. Factors Influencing Chemical Shifts of Skeletal Atoms. *Chem. Rev.* **1992**, *92*, 325-362.

(34) (a) Lee, G. M.; Bowes, E. G.; Vogels, C. M.; Decken, A.; Westcott, S. A. Cyclisations of Alkynoic Acids using Copper(I) Arylspiroborate Complexes. *Tetrahedron* **2019**, *75*, 2106-2112. (b) Riddlestone, I. M.; Kraft, A.; Schaefer, J.; Krossing, I. Taming the Cationic Beast: Novel Developments in the Synthesis and Application of Weakly Coordinating Anions. *Angew. Chem. Int. Ed.* **2018**, *57*, 13982-14024.

(35) See the supporting information for experimental details and spectra.

(36) For the complete picture, see Figure S21. Notably, the solid-state structure of **3a** led to the second most stable isomer (**3a^{DFT}**) while the diastereomer **3a$'^{DFT}$** was most stable.

(37) LiOtBu was also used in attempts to isolate the lithium spiroboralactonate following the salt metathesis reaction. However, as with the NaOtBu, isolation was not possible.

(38) k_{2nd} is defined as $k_{2nd} = (k_{obs})/[\mathbf{2x}]$, given that CO_2 is in large excess.

(39) To the best of our knowledge, there have been no well-defined complementary experimental/computational studies of Cu^{I}-catalyzed benzyl/alkyl carboxylation. For computational studies, see: references 10e, 26-28

(40) (a) Zhao, H.; Lin, Z.; Marder, T. B. Density Function Theory Studies on the Mechanism of the Reduction of CO_2 to CO Catalyzed by Copper(I) Boryl Complexes. *J. Am. Chem. Soc.* **2006**, *128*, 15637-15643. (b) Dang, L.; Zhao, H.; Lin, Z.; Marder, T. B. DFT Studies of Alkene Insertions into Cu-B Bonds in Copper(I) Boryl Bonds. *Organometallics* **2007**, *26*, 2824-2832. (c) Dang, L.; Lin, Z. DFT Studies on the Carboxylation of Arylboronate Esters with CO_2 Catalyzed by Copper(I) Complexes. *Organometallics* **2010**, *29*, 917-927.

(41) For comparisons of calculated Hammett trends using M06, B3LYP, and B97D3 functionals, see: Figure S15 and Tables S2-S3.

(42) For recent studies of copper(I) catalyzed processes using B3LYP functional, see: (a) Fan, T.; Sheong, F. K.; Lin, Z. DFT Studies on Copper-Catalyzed Hydrocarboxylation of Alkynes Using CO_2 and Hydrosilanes. *Organometallics* **2013**, *32*, 5224-5230. (b) Dang, L.; Lin, Z. DFT Studies on the Carboxylation of Arylboronate Esters with CO_2 Catalyzed by Copper(I) Complexes. *Organometallics* **2010**, *29*, 917-927. (c) Zhao, H.; Dang, L.; Marder, T. B.; Lin, Z. DFT Studies on the Mechanism of the Diboration of Aldehydes Catalyzed by Copper(I) Boryl Complexes. *J. Am. Chem. Soc.* **2008**, *130*, 5586-5594. (d) Dang, L.; Zhao, H.; Lin, Z. DFT Studies of Alkene Insertions into Cu-B Bonds in Copper(I) Boryl Complexes. *Organometallics* **2007**, *26*, 2824-2832. (e) Zhao, H.; Lin, Z.; Marder, T. B. Density Functional Theory Studies on the Mechanism of the Reduction of CO_2 to CO Catalyzed by Copper(I) Boryl Complexes. **2006**, *128*, 15637-15643.

(43) B3LYP led to systematic over-estimation of the free energy barrier for each carboxylation in the series when compared to the experimentally derived values, an observation consistent with similar previous DFT studies: Collins, L. R.; Rajabi, N. A.; Macgregor, S. A.; Mahon, M. F.; Whittlesey, M. K. Experimental and Computational Studies of the Copper Borate Complexes [(NHC)Cu($HBEt_3$)] and [(NHC)Cu($HB(C_6F_5)_3$)]. *Angew. Chem. Int. Ed.* **2016**, *128*, 15768-15772.

(44) The inclusion of dispersion corrections was also considered using B97D3. Results showed similar trends to that obtained with dispersion uncorrected M06. Grimme, S.; Hansen, A.; Brandenburg, J. G.; Bannwarth, C. Dispersion-Corrected Mean-Field Electronic Structure Methods. *Chem. Rev.* **2016**, *116*, 5105-5154.

(45) For select reviews on metal-π-benzyl complexes and their reactivity, see: (a) Song, J.; Liu, Q.; Liu, H; Jiang, X. Recent Advances in Palladium-Catalyzed Carboxylation with CO_2. *Eur. J. Org. Chem.* **2018**, *6*, 696-713. (b) Trost, B. M.; Czabaniuk, L. C. Structure and Reactivity of Late Transition Metal η^3-Benzyl Complexes. *Angew. Chem. Int. Ed.* **2014**, *53*, 2826-2851.

(46) For selected works on utilization of Lewis basic additives in catalysis, see: (a) Hong, L.; Sun, W.; Yang, D.; Li, G.; Wang, R. Additive Effects on Asymmetric Catalysis. *Chem. Rev.* **2016**, *116*, 4006-4123, and references therein. (b) Balaji, P. V.; Brewitz, L.; Kumagai, N.; Shibasaki, M. Achiral Trisubstituted Thioureas as Secondary Ligands to Cu^{I} Catalysts: Direct Catalytic Asymmetric Addition of α-Fluoronitriles to Imines. *Angew. Chem. Int. Ed.* **2019**, *131*, 2670-2674. (c) Xu-Xu, Q. F.; Zhang, X.; You, S. L. Enantioselective Synthesis of 4-Aminotetrahydroquinolines via 1,2-Reductive Dearomatization of Quinolines an Copper(I) Hydride-Catalyzed Asymmetric Hydroamination. *Org. Lett.* **2019**, *21*, 5357-5362. (d) Lu, D. F.; Zhu, C. L.; Xu, H. Copper(I)-catalyzed diastereoselective Hydroxytrifluoromethylation of Dienes Accelerated by Phosphine Ligands. *Chem.*

Sci. **2013**, *4*, 2478-2482. (e) Zhao, D.; Mao, L.; Yang, D.; Wang, R. Catalytic Asymmetric Construction of Tetrasubstituted Carbon Stereocenters by Conjugate Addition of Dialkyl Phosphine Oxides to β,β-Disubstituted α,β-Unsaturated Carbonyl Compounds. *Chem. Comm.* **2012**, *48*, 889-891. (f) Jin, W.; Li, X.; Wan, B. Highly Diastereo- and Enantioselective Copper(I)-Catalyzed Henry Reaction Using a Bis(sulfonamide)-Diamine Ligand. *J. Org. Chem.* **2011**, *76*, 484-491. (h) Zhao, D.; Mao, L.; Wang, Y.; Yang, D.; Zhang, Q.; Wang, R. Catalytic Asymmetric Hydrophosphinylation of α,β-Unsaturated N-Acylpyrroles: Application of Dialkyl Phosphine Oxides in Enantioselective Synthesis of Chiral Phosphine Oxides or Phosphines. *Org. Lett.* **2010**, *12*, 1880-1882.

(47) (a) Xu-Xu, Q. F.; Zhang, X.; You, S. L. Enantioselective Synthesis of 4-Aminotetrahydroquinolines via 1,2-Reductive Dearomatization of Quinolines and Copper(I) Hydride-Catalyzed Asymmetric Hydroamination. *Org. Lett.* **2019**, *21*, 5357-5362. (b) Bandar, J. S.; Pirnot, M. T.; Buchwald, S. L. Mechanistic Studies Lead to Dramatically Improved Reaction Conditions for the Cu-Catalyzed Asymmetric Hydroamination of Olefins. *J. Am. Chem. Soc.* **2015**, *137*, 14812-14818. (c) Lipshutz, B. H.; Noson, K.; Chrisman, W.; Lower, A. Asymmetric Hydrosilylation of Aryl Ketones Catalyzed by Copper Hydride Complexed by Nonracemic Biphenyl Bis-phosphine Ligands. *J. Am. Chem. Soc.* **2003**, *125*, 8779-8789.

(48) Lotito, K. J.; Peters, J. C. Efficient Luminescence from Easily Prepared Three-Coordinate Copper(I)Arylamidophosphines. *Chem. Commun.* **2010**, *46*, 3690-3692.

(49) Batsanov, S. S. Van der Waals Radii of Elements. *Inorg. Mater.* **2001**, *37*, 1031-1046.

(50) Dherbassy, Q.; Djukic, J. P.; Wencel-Delord, J.; Colobert, F. Two Stereoinduction Events in One C-H Activation Step: A Route towards Terphenyl Ligands with Two Atropisomeric Axes. *Angew. Chem. Int. Ed.* **2018**, *57*, 4668-4672.

(51) Jurkauskas, V.; Sadighi, J. P.; Buchwald, S. L. The Conjugate Reduction of α,β-Unsaturated Carbonyl Compounds Catalyzed by a Copper Carbene Complex. *Org. Lett.* **2003**, *5*, 2417-2420.

(52) APEX3: Crystallographic Software Package for Single Crystal Data Collection, Reduction and Preparation, version 2016.9-0; Bruker AXS: Madison, WI, 2016.

(53) Sheldrick, G. M. SHELXL-2014: Crystallographic Software Package; Bruker AXS, Inc.: Madison, WI, 2014.

(54) Gaussian 16, Revision B.01, M. J. Frisch, G. W. Trucks, H. B. Schlegel, G. E. Scuseria, M. A. Robb, J. R. Cheeseman, G. Scalmani, V. Barone, G. A. Petersson, H. Nakatsuji, X. Li, M. Caricato, A. V. Marenich, J. Bloino, B. G. Janesko, R. Gomperts, B. Mennucci, H. P. Hratchian, J. V. Ortiz, A. F. Izmaylov, J. L. Sonnenberg, D. Williams-Young, F. Ding, F. Lipparini, F. Egidi, J. Goings, B. Peng, A. Petrone, T. Henderson, D. Ranasinghe, V. G. Zakrzewski, J. Gao, N. Rega, G. Zheng,W. Liang, M. Hada, M. Ehara, K. Toyota, R. Fukuda, J. Hasegawa, M. Ishida, T. Nakajima, Y. Honda, O. Kitao, H. Nakai, T. Vreven, K. Throssell, J. A. Montgomery, Jr., J. E. Peralta, F. Ogliaro, M. J. Bearpark, J. J. Heyd, E. N. Brothers, K. N. Kudin, V. N. Staroverov, T. A. Keith, R. Kobayashi, J. Normand, K. Raghavachari, A. P. Rendell, J. C. Burant, S. S. Iyengar, J. Tomasi, M. Cossi, J. M. Millam, M. Klene, C. Adamo, R. Cammi, J. W. Ochterski, R. L. Martin, K. Morokuma, O. Farkas, J. B. Foresman, and D. J. Fox, Gaussian, Inc., Wallingford CT, 2016.

(55) Zhao, Y.; Truhlar, D. G. The M06 Suite of Density Functionals for Main Group Thermochemistry, Thermochemical Kinetics, Noncovalent Interactions, Excited States, and Transition Elements: Two New Functionals and Systematic Testing of Four M06-class Functionals and 12 Other Functionals. *Theor. Chem. Acc.* **2008**, *120*, 215–241.

(56) (a) McLean, A. D.; Chandler, G. S. Contracted Gaussian-Basis Sets for Molecular Calculations. 1. 2nd Row Atoms, Z=11-18. *J. Chem. Phys.* **1980**, *72*, 5639-5648. (b) Raghavachari, K.; Binkley, J. S.; Seeger, R.; Pople, J. A. Self-Consistent Molecular Orbital Methods. 20. Basis Set for Correlated Wave-Functions," *J. Chem. Phys.*, **1980**, *72*, 650-6554. (c) Wachters, A. J. H. Gaussian Basis Set for Molecular Wavefunctions Containing Third-Row Atoms. *J. Chem. Phys.*, **1970**, *52*, 1033. (d) Hay, P. J. Gaussian Basis Sets for Molecular Calculations – Representation of 3D Orbitals in Transition-Metal Atoms. *J. Chem. Phys.*, **1977**, *66,* 4377-4384. (e) Raghavachari, K.; Trucks, G. W. Highly Correlated Systems: Excitation Energies of First Row Transition Metals Sc-Cu. *J. Chem. Phys.*, **1989**, *91*, 1062-65.

(57) (a) Becke, A. D. Density Functional Calculations of Molecular Bond Energies. J. Chem. Phys. 1986, 84, 4524–4529. (b) Becke, A. D. Density-Functional Thermochemistry. III. The Role of Exact Exchange. J. Chem. Phys. 1993, 98, 5648–5652. (c) Lee, C.; Yang, W.; Parr, R. G. Development of the Colle-Salvetti Correlation-Energy Formula into a Functional of the Electron Density. Phys. Rev. B: Condens. Matter Mater. Phys. 1988, 37, 785–789.

(58) Grimme, S.; Antony, J.; Ehrlich, S.; Krieg, H. A consistent and accurate *ab initio* parametrization of density functional dispersion correction (DFT-D) for the 94 elements H-Pu. *J. Chem. Phys.* **2010, *132***, 154104.(59) (a) Fukui, K. Formulation of the reaction coordinate. *J. Phys. Chem.* **1970**, *74*, 4161–4163. (b) Fukui, K. The Path of Chemical Reactions - the IRC Approach. *Acc. Chem. Res.* **1981**, *14*, 363–368.

(60) Marenich, A. V.; Cramer, C. J.; Truhlar, D. G. Universal Solvation Model based on Solute Electron Density and a Continuum Model of the Solvent Defined by the Bulk Dielectric Constant and Atomic Surface Tensions. *J. Phys. Chem. B*, **2009**, *113*, 6378-96.

(61) Jmol: an open-source Java viewer for chemical structures in 3D. http://www.jmol.org/

TOC Graphic